PROCESS DEVELOPMENT, KINETIC MODELING, AND TECHNO-ECONOMIC ANALYSIS OF ENZYMATIC CELLULOSE HYDROLYSIS

A Dissertation

by

CHAO LIANG

Submitted to the Office of Graduate and Professional Studies of
Texas A&M University
in partial fulfillment of the requirements for the degree of

DOCTOR OF PHILOSOPHY

Chair of Committee,	Mark Holtzapple
Committee Members,	Mahmoud El-Halwagi
	Ahmad Hilaly
	Sergio Capareda
Head of Department,	Arul Jayaraman

December 2019

Major Subject: Chemical Engineering

ABSTRACT

Countercurrent saccharification is a promising way to minimize enzyme loading while obtaining high conversions and product concentrations. However, in countercurrent saccharification experiments, 3–4 months are usually required to acquire a single steady-state data point. To save labor and time, simulation of this process is necessary to test various reaction conditions and determine the optimal operating point. Previously, a suitable kinetic model for countercurrent saccharification has never been reported.

To simulate countercurrent saccharification, a kinetic model that could satisfactorily predict batch saccharification under various reaction conditions is necessary. In this study, the HCH-1 model was modified to extend its application to integrated enzymatic hydrolysis; it performed well when predicting 10-day cellulose hydrolysis at various experimental conditions. Comparison with the literature models showed that the modified HCH-1 model provided the best fit for batch enzymatic cellulose hydrolysis.

The Continuum Particle Distribution Modeling (CPDM) was applied to simulate countercurrent saccharification of α-cellulose. The modified HCH-1 model was used as the governing equation in the CPDM model. When validated against experimental countercurrent saccharification data, it predicts experimental glucose concentrations and conversions with the average errors of 3.5% and 4.7%, respectively. CPDM predicts conversion and product concentration with varying enzyme-addition location, total stage

number, enzyme loading, liquid residence time, and solids loading rate. In addition, countercurrent saccharification was compared to batch saccharification at the same conversion, product concentration, and reactor volume. Results show that countercurrent saccharification is particularly beneficial when the product concentration is low.

Techno-economic analysis was performed for cellulosic sugar production. Various reaction conditions, equipment materials, enzyme unit prices, and return on investments (ROIs) were considered. Excluding feedstock cost but including utility cost (dewatering), enzyme cost, depreciation, and fixed operating costs, using geomembrane reactor and carbon steel mechanical vapor recompression (MVR) evaporators, the estimated minimum selling prices are $0.079/kg glucose with commercial CTec2 cellulase ($6.27/kg protein) and $0.064/kg glucose with on-site cellulase production ($4.24/kg protein). Compared to batch saccharification at the same reaction conditions, equipment materials, and enzyme unit prices, countercurrent saccharification significantly reduces the cost of cellulosic sugar production.

DEDICATION

To my family: parents, husband, daughter, and cat.

ACKNOWLEDGEMENTS

I am extremely grateful to my advisors Dr. Mark T. Holtzapple and Dr. M. Nazmul Karim for their guidance and generous financial support. This work could not be finished without their instruction and constant encouragement. It's really my honor to work with them. I would also like to thank my committee member Dr. Sergio Capareda, Dr. Mahmoud El-Halwagi, and Dr. Ahmad Hilaly for their help and support throughout this research.

I would like to thank Dr. Zivko Nikolov for his comments and support for my research. Thanks also go to my colleges Kefan Yang, Haoran Wu, Shen-chun Hsu, Opeyemi Olokede, Kejia Liu, Pallavi Kumari, Dr. Ju Huang, Dr. Sagar Lonkar, Dr. Austin Bond, Dr. Pratik Darvekar, Dr. Xinghua Pan, Dr. Jonathan Raftery, Dr. Melanie DeSessa, Dr. Chiranjivi Botre, and Dr. Zhihong Fu for their kind assistance and friendship.

I would also like to convey my thanks to Toni Alvarado, Ashley Henley, Terah Cooper, Crystal Ray for their kind assistance and to all the student workers who helped me with my experiments. Special thanks to Hatake Kakashi and Roger Federer for enriching my life.

Finally, I am grateful to my parents Huiqing Liang and Ronghui Zhou for their professional instruction, unconditional love, and support. Thanks also go to my husband Chao Gu, my daughter Enthalpy Gu, and my cat Lvrouhuoshao for their love and company.

CONTRIBUTORS AND FUNDING SOURCES

Contributors

This work was supervised by a dissertation committee consisting of Professor Mark Holtzapple, Professor Mahmoud El-Halwagi, and Professor Ahmad Hilaly of the Department of Chemical Engineering and Professor Sergio Capareda of the Department of Biological and Agricultural Engineering.

The experimental data of countercurrent saccharification with α-cellulose was provided by Agustin N. Zentay. All other work conducted for the dissertation was completed by the student independently.

Funding Sources

This work was supported by the Michael O'Connor Chair II (Dr. M. Nazmul Karim) Endowment and Dr. Mark Holtzapple's Funding. The open access publishing fees for the two papers "Development of modified HCH-1 kinetic model for long-term enzymatic cellulose hydrolysis and comparison with literature models" (Chapter III) and "Kinetic modeling of countercurrent saccharification" (Chapter IV) were covered by the Texas A&M University Open Access to Knowledge Fund (OAKFund), supported by the University Libraries and the Office of the Vice President for Research.

NOMENCLATURE

Aceq	Acetic Acid Equivalents
AIC	Akaike Information Criterion
AICc	Corrected Akaike Information Criterion
CPDM	Continuum Particle Distribution Modeling
CSTR	Continuous Stirred Tank Reactor
DI Water	Deionized Water
FCI	Fixed Capital Investment
HPLC	High-performance Liquid Chromatography
IC	Installed Costs
LRT	Liquid Residence Time
mg/g	mg protein added/g dry biomass added
MVR Evaporators	Mechanical Vapor Recompression Evaporators
NREL	National Renewable Energy Laboratory
PFR	Plug Flow Reactor
ROI	Return on Investment
SLR	Solids Loading Rate
SSE	Sum of Square Errors
TDC	Total Direct Costs
WC	Working Capital

TABLE OF CONTENTS

Page

LIST OF FIGURES

Page

LIST OF TABLES

Page

CHAPTER I

INTRODUCTION

Currently, fossil fuels such as natural gas, oil, and coal are the main sources of energy and chemicals. However, the shortage of fossil fuels and their impact on the environment are increasingly severe. Developing alternative energy resources is necessary and urgent. Biomass is a leading possible replacement for petroleum-derived liquid transportation fuels, which captures solar energy and fixes carbon through photosynthesis (Klass, 2004; Darvekar et al., 2019). It is the only renewable energy resource that can be directly converted to liquid fuels and chemicals. The largest biomass feedstock is lignocellulose, which is found globally in many forms. Converting lignocellulose into biofuels could relieve shortages of liquid fuels and reduce dependence on fossil energy.

In the United States, ethanol is the dominant biofuel, which is usually produced from corn, an important food for animals and humans. To prevent food shortages, cellulosic ethanol is an attractive alternative. Generally, there are four major steps for cellulosic ethanol production: pretreatment, hydrolysis, fermentation, and separation. Among these processes, hydrolysis accounts for a large portion (~30%) of the total costs (Wallace et al., 2005). To compete with corn ethanol and petroleum-derived gasoline, enzymatic hydrolysis needs optimization and cost reduction (Wooley et al., 1999).

Batch processing is widely used in enzymatic hydrolysis; however, it cannot fully use substrate because as substrate is hydrolyzed, biomass becomes less reactive (Yang et al., 2006; Kumar and Wyman, 2009a) while the enzymes become increasingly

inhibited by accumulated product; therefore, high enzyme loadings are usually required to reach high conversions. To overcome these obstacles, countercurrent enzymatic saccharification was developed, where the least reactive biomass contacts the lowest glucose concentration and the product is removed continuously from the system, thus reducing product inhibition. This approach more fully utilizes enzymes and therefore reduces the enzyme loadings and lowers the cost of sugar and biofuel production.

In countercurrent saccharification experiments, 3 to 4 months are usually required to acquire a single steady-state data point. To save labor and time, simulation of this process is necessary to test various reaction conditions and determine the optimal operating point. Previously, a suitable kinetic model for countercurrent saccharification has never been reported.

The aims of this study are the followings:

- Develop a kinetic model that could satisfactorily predict batch saccharification at various conditions, which is the basis of the simulation of countercurrent saccharification.
- Develop a kinetic model that could satisfactorily predict countercurrent saccharification at various conditions.
- Conduct techno-economic analysis to determine the operating point of countercurrent saccharification that has the lowest cost of cellulosic sugar production.

CHAPTER II

COUNTERCURRENT SACCHARIFICATION

Introduction

Countercurrent systems are widely used in liquid-liquid extraction (Martin and Synge, 1941), heat exchange (Uozu et al., 1989), and other systems. It also has great potential to improve enzymatic saccharification by fully utilizing enzymes resulting in higher sugar yields than batch saccharification thus reducing the cost of sugar and biofuel production.

The benefits of countercurrent saccharification have been explored in several previous studies (Fox et al., 1983; Jeffries and Schartman, 1999). These previous studies employed only three stages; in contrast, this study uses many more stages (≥ 8 stages). Further, this study adds enzymes to a fixed, intermediate stage rather than a moving, terminal stage (Jeffries and Schartman, 1999, Zentay et al., 2016). At steady state, performance of countercurrent saccharification is compared to batch saccharification.

Materials and Methods

Materials

Substrate

Three kinds of substrates were used in the countercurrent saccharification experiments:

(1) a-Cellulose (Sigma Aldrich C8002-5KG). Compositional analysis showed that the substrate contained glucan 78.5% and xylan 14.4% (Zentay et al., 2016).

(2) Lime-pretreated corn stover. The literature shows that lime pretreatment removes lignin and acetyl groups effectively (Chang and Holtzapple, 2000, Kim 2005). In this study, lime pretreatment procedures mainly followed the oxidative long-term pretreatment method (Sierra et al., 2009). Raw corn stover (glucan 32.6% and xylan 19.3%, lignin 11.7%), $Ca(OH)_2$, and water were placed in the pretreatment vessel with the following conditions: 10 kg water/kg dry biomass and 0.15 kg $Ca(OH)_2$/kg dry biomass. The pretreatment time was 30 days with temperature 50°C. Then the pretreated corn stover was washed, dried, and used as the substrate for enzymatic hydrolysis. Compositional analysis showed that the substrate contained glucan 45.3%, xylan 18.1%, and lignin 8.6% (Liang, 2015; Sagar et al., 2017).

(3) Lime + shock pretreated corn stover. The lime-pretreated corn stover was further shock treated in a 20-L vessel with a conical section and run-up tube. The shock vessel was loaded with 1.4 kg dry corn stover and 14 L water (including water in biomass). Stoichiometric H_2 and O_2 were added to the head space of the apparatus and ignited using a glow plug. Detonation causes a rapid pressure increase to 12 MPa within 19 ms. The resulting shock wave transferred through the aqueous slurry and mechanically disrupted the structure of corn stover. Finally, the lime + shock pretreated biomass slurry was air dried so it could be safely stored as a substrate for enzymatic hydrolysis. Compared with other mechanical treatments, shock pretreatment has the advantages of low cost (<$5/tonne) and the potential to scale up (Holtzapple, 2014). Compositional analysis showed that the substrate contained glucan 44.3%, xylan 19.6%,

and lignin 10.4% (Liang et al., 2017; Sagar et al., 2017, Falls et al., 2019; Falls et al., 2017a; Falls et al., 2017b; Madison et al., 2017).

Enzyme Solutions

The enzyme used for the experiments with α-cellulose was Novozymes Ctec2 (lot # VCPI 0007), a blend of aggressive cellulases with high levels of β-glucosidases and hemicellulases. The protein concentration of the enzyme solution was determined to be 294 mg protein/mL with Pierce BCA assay (Zentay., 2016).

The enzymes used for the experiments with lime-pretreated and lime + shock treated corn stover were Novozymes CTec3 and HTec3. CTec3 is Novozymes's newest commercial enzyme product for effective hydrolysis of cellulose. It contains proficient cellulase components boosted by proprietary enzyme activities and a new array of hemicellulase activities (Novozymes, 2012a). HTec3 is the newest commercial enzyme product from Novozymes for effective hydrolysis of insoluble and soluble hemicelluloses (Novozymes, 2012b). The protein concentrations of CTec3 and HTec3 solutions were determined to be 326 and 243 mg protein/mL with Pierce BCA assay (Liang et al., 2017; Sagar et al., 2017; Liang, 2015).

Citrate Buffer

To maintain relatively high enzyme activity, citrate buffer (0.1 M, pH 4.8) was used in all saccharification experiments.

Antibiotics

To prevent the growth of contaminating microorganisms that could consume produced sugars, an antibiotic cocktail was added. To prepare the solutions, tetracycline powder was dissolved in an aqueous solution of 70% ethanol at 10 g/L and cycloheximide powder was dissolved in deionized (DI) water at 10 g/L.

Countercurrent Saccharification

Figure 2-1 shows the system diagram for an eight-stage countercurrent saccharification. To begin the countercurrent experiment, all the stages (Nalgene centrifuge bottles, 1 L, Fisher catalog # 05-562-26) were loaded with 250 g materials, including 25 g dry substrate, 125 mL citrate buffer, 2 mL tetracycline solutions, 1.5 mL cycloheximide solutions, and given amounts of enzyme solution and DI water. (*Note:* The density of all liquid materials was assumed to be 1 g/cm^3.) The bottles were placed in 4-in-ID PVC pipes and axially rotated at 2 rpm by a Wheaton Roller Apparatus located in the custom-made incubator at 50°C. The transfers were performed every 48 h. In every transfer, each bottle was centrifuged to achieve phase separation of liquid and solid wet cake (70–80% moisture content). The mass of each phase and the pH of the liquid phase were measured. A liquid sample (1 mL) was taken from every bottle and analyzed by HPLC to determine when the system reached steady state. All the liquid was moved from "back" to "front" and the solid phases were moved in the opposite direction. The amount of solid phase transferred was calculated to ensure each stage had the same amount of wet cake after each transfer. Then, 10 g dry substrate was loaded in the first

stage and 90 mL liquid consisting of 50 mL citrate buffer and 40 mL DI water was added to the last stage. Antibiotic solutions (0.4 mL tetracycline solution and 0.3 mL cycloheximide solution) were introduced to every stage and the desired amount of enzymes was added to a specific location. When the sugar concentrations from each stage did not show significant change over a relatively long time (e.g., 15 days), the system was determined to reach steady state. Table 2-1 summarizes the operating parameters of countercurrent saccharification experiments (Zentay et al., 2016; Sagar et al., 2017; Liang et al., 2017).

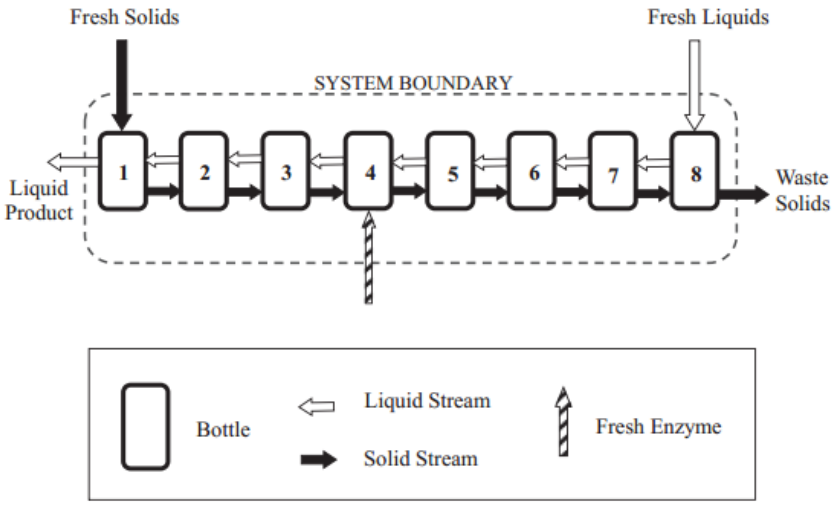

Figure 2-1 System diagram of countercurrent saccharification (Reprinted from Zentay et al., 2016).

Table 2-1 Operating parameters of countercurrent saccharification experiments

Train	**1**	**2**	**3**	**4**	**5**	**6**	**7**
Substrate	α-Cellulose		Lime-pretreated corn stover		Lime + shock treated corn stover		
Enzyme type and loading	CTec2 2 mg/g	CTec2 5 mg/g	CTec3 1 mg/g	CTec3 1 mg/g + HTec3 1 mg/g	CTec3 1 mg/g	CTec3 1 mg/g + HTec3 1 mg/g	CTec3 2 mg/g + HTec3 2 mg/g
Total reaction time (days)	24	42	120	100	120	100	80
Total stage number	8	8	16	16	16	16	16
Enzyme-addition location (stage number)	4	5	4	4	4	4	4
Target wet cake amount (g)	85	80	90	90	90	90	90
Reference	Zentay et al., 2016		Sagar et al., 2017		Liang et al., 2017		

Note: mg/g = mg protein added/g dry biomass added.

The glucose conversion was determined as the ratio of glucose exiting the countercurrent system to the equivalent glucose entering the system in each transfer (*Note:* Cellobiose was not considered in this study because the enzymes CTec2 and CTec3 contain high levels of β-glucosidase that rapidly convert the produced cellobiose into glucose.) The glucose exiting the system was the summation of glucose exiting from the first and last stages, and glucose in liquid samples from all stages. The equivalent glucose entering the system was from the substrate added to the first stage.

Results and Discussion

Countercurrent Saccharification

Figure 2-2 shows the glucose concentrations as a function of stage number and

time (Train 2). At the beginning, the glucose concentration significantly changes until it eventually stabilizes when the system reaches steady state. Similar trends were observed for glucose concentration in other trains. More experimental results are shown in Zentay et al. (2016), Sagar et al. (2017), and Liang et al. (2017).

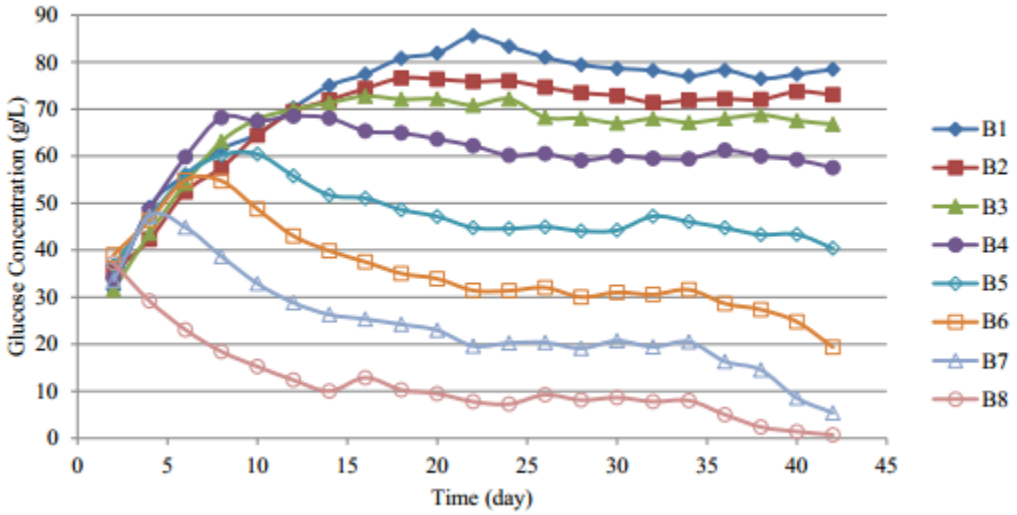

Figure 2-2 Glucose concentrations as a function of time and stage (bottle) number (Train 2, Reprinted from Zentay et al., 2016).

Comparison of Countercurrent to Batch

To evaluate efficacy, countercurrent results are compared with batch reactions with typical reaction time (5 days). To achieve a given steady-state conversion in countercurrent saccharification, the corresponding enzyme loading in batch saccharification was determined. Table 2-2 compares the enzyme requirements for batch and countercurrent saccharifications and the factor reduction.

Table 2-2 Comparison of enzyme requirements for batch and countercurrent saccharification

Train		**1**	**2**	**3**	**4**	**5**	**6**	**7**
Glucose conversion (%)		56	88	61	67	64	72	82
Total enzyme loading (mg/g)	**Countercurrent**	2.0	5.0	1.0	2.0	1.0	2.0	4.0
	Batch (5-day)	16.0	84.0	1.6	2.8	1.9	2.8	3.2
Factor reduction		8.0	16.8	1.6	1.4	1.9	1.4	0.8

As shown in Table 2-2, using α-cellulose as substrate, to achieve the same glucan conversion, as compared to typical 5-day batch saccharification, countercurrent saccharification reduced enzyme requirements up to 16.8 times. The great reduction resulted from the inherent benefits of countercurrent saccharification as well as a longer residence time. Using lime-pretreated corn stover as substrate, to achieve the same glucan conversion, as compared to batch, countercurrent saccharification reduced enzyme requirements up to 1.6 times. Using lime + shock treated corn stover as substrate, to achieve the same glucan conversion, as compared to batch, countercurrent saccharification reduced enzyme requirements up to 1.9 times. Compared to α-cellulose, the results with pretreated corn stover show a much smaller factor reduction indicating that lignin may bind enzymes unproductively.

Conclusions

Multi-stage countercurrent saccharifications were performed with lignocellulose model compound (α-cellulose), lime-pretreated corn stover, and lime + shock treated corn stover. Compared to batch saccharification, to reach a given glucan conversion, countercurrent saccharification reduced enzyme loadings up to 16.8 times using α-cellulose. Compared to batch saccharification, to reach a given glucan conversion, countercurrent saccharification reduced enzyme loadings up to 1.6 and 1.9 times using lime-pretreated and lime + shock treated corn stover, respectively. Countercurrent saccharification shows great promise as a way to minimize enzyme loading while maintaining high conversions.

CHAPTER III

KINETIC MODELING OF BATCH SACCHARIFICATION[1]

Introduction

In countercurrent saccharification, the reaction in every stage between transfers can be considered as batch saccharification; therefore, to get a satisfactory prediction of countercurrent saccharification, a kinetic model that can accurately describe batch saccharification under various reaction conditions is necessary.

During the last several decades, various theoretical and empirical models have been developed to simulate batch enzymatic hydrolysis of cellulose (Holtzapple et al., 1984; Kadam et al., 2004; Fenila and Shastri, 2016). Because they lack a theoretical foundation, empirical models cannot be applied beyond the range of the data; therefore, this study only focuses on mechanistic (and semi-mechanistic) models.

In 1984, Holtzapple *et al.* (1984) proposed a generalized mechanistic model for cellulose hydrolysis termed the HCH-1 (Holtzapple-Caram-Humphrey-1) model. Figure 3-1 shows the reaction mechanism of the HCH-1 model (Holtzapple et al., 1984). As shown in the figure, free enzyme (E^f) adsorbs onto a free cellulose site (G_x^f) to become adsorbed enzyme (E^a), and then complexes with the cellulose to become enzyme-substrate complex (EG_x). This complex catalyzes the hydrolysis of the cellulose site to obtain soluble product (G_s) with reaction rate k**.** All enzyme species can complex with

[1] The content of this chapter is from: Liang, C., Gu, C., Raftery, J., Karim, M.N., Holtzapple, M., 2019. Development of modified HCH-1 kinetic model for long-term enzymatic cellulose hydrolysis and comparison with literature models. Biotechnology for Biofuels. 12: 34.

product to become inhibited enzyme (G_sE^f, G_sE^a, and G_sEG_x). For simplicity, the product binding constant (β) is assumed to be the same for all enzyme species. Also, the adsorption constant (δ) and the complexing constant (η) are assumed not to be affected by the binding of product to the enzyme (Holtzapple et al., 1984).

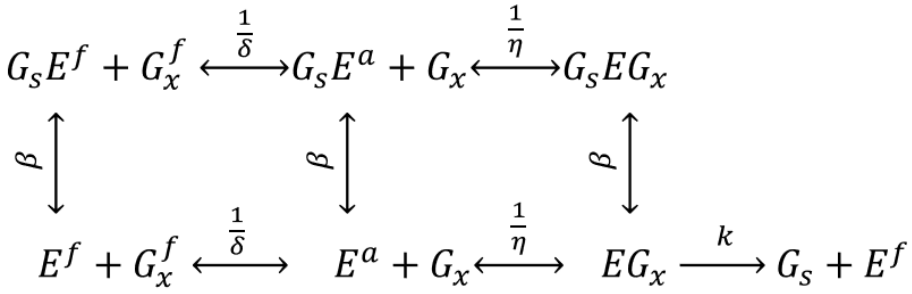

Figure 3-1 Reaction mechanism for the HCH-I model (Holtzapple et al., 1984).

The rate-limiting step is the hydrolysis; therefore, the reaction velocity (V) is proportional to the concentration of uninhibited enzyme-substrate complex (EG_x). To express the reaction velocity in terms of known variables, substitutions can be made for EG_x using material balances of substrate and enzyme species thus yielding the HCH-1 model (Eq. 3-1). The detailed model development is described in Holtzapple et al. (1984).

$$V = \frac{\kappa[G_x][E]i}{\alpha + \varphi[G_x] + \varepsilon[E]}$$

$$i = \frac{1}{1 + \beta_1[G_1] + \beta_2[G_2]}$$

$$\varphi = \frac{[G_x] - \alpha - \varepsilon[E] + \sqrt{([G_x] - \alpha - \varepsilon[E])^2 + 4\alpha[G_x]}}{2[G_x]} \qquad (3\text{-}1)$$

where,

G_x is the cellulose concentration (g/L, equivalent to glucose)

G_1 is the glucose concentration (g/L)

G_2 is the cellobiose concentration (g/L, equivalent to glucose)

E is the enzyme concentration (g/L)

α is the lumped adsorption constant ($\alpha = \frac{\eta\delta}{\eta+1}$, g/L)

κ is the lumped kinetic constant ($\kappa = \frac{k}{\eta+1}$, h^{-1})

β_1 is the glucose binding constant (L/g)

β_2 is the cellobiose binding constant (L/g)

ε is the number of cellulose sites covered by adsorbed or complexed enzyme (dimensionless)

i is the fraction of total enzyme that is active (dimensionless)

φ is the fraction of total cellulose sites which are free (dimensionless).

Unlike the classic Michaelis–Menten model, the HCH-1 model includes a parameter ε that describes the number of reactive sites covered by the enzymes (Holtzapple et al., 1984; Brown et al., 2010). Furthermore, the HCH-1 model includes non-competitive inhibition by sugar products.

Unlike empirical models that apply only in the range where the data were taken, the HCH-1 model is mechanistic (Figure 3-1) and therefore has broader applicability.

As a mechanistic model, it applies to individual enzyme species; however, it has also been applied successfully to an enzyme cocktail in which the mixture is treated as a single "lumped" enzyme. Using initial-rate data for pretreated biomass hydrolyzed by an enzyme cocktail, Brown *et al*. (2010) compared mechanistic models and showed that the HCH-1 model provided the best fit to experimental data.

Previous studies show that at high degrees of conversion, the hydrolysis rate drops by two to three orders of magnitude (Bommarius et al., 2008; Hong et al., 2007). The following factors contribute to the decreasing hydrolysis rates: (1) enzyme deactivation, (2) product inhibition, (3) decreased substrate reactivity, (4) decreased substrate accessibility, and (5) decreased synergism between cellulases (Bansal et al., 2009). In short-term enzymatic hydrolysis, these factors are not important and therefore are usually not incorporated into models that predict initial rates. However, in long-term batch saccharification, the reaction time is usually three to five days. As the reaction proceeds, the coefficients in short-term enzymatic hydrolysis models, such as HCH-1, may change because of the enumerated factors above. To describe long-term integrated enzymatic hydrolysis, initial-rate models must be modified.

In this study, the original HCH-1 model was modified to describe 10-day enzymatic cellulose hydrolysis with commercial enzyme cocktail CTec2. The HCH-1 mechanism (Figure 3-1) applies to individual enzymes in the cocktail; however, modeling each enzyme component is exceedingly complex. Understanding the kinetics of each enzyme component would be useful when optimizing the cocktail; however, this study uses a cocktail with defined components. Our approach is to treat the enzyme

cocktail as a single “lumped” enzyme; hence, the resulting “lumped” parameters reflect the collective kinetics of the cocktail, not the individual components. To describe long-term enzymatic hydrolysis, this study investigates the relationships between the “lumped” parameters in the HCH-1 model and substrate conversion. The sensitivities of parameters in the modified model were analyzed. Additionally, literature models for long-term (>48 h) enzymatic hydrolysis were summarized and compared to the modified HCH-1 model.

Materials and Methods

Materials

Substrate

In this chapter, the substrate used for all experiments was α-cellulose (Sigma-Aldrich, C8002). Compositional analysis showed that the substrate contained glucan 78.5% and xylan 14.4% (Zentay et al., 2016).

Enzyme

The enzyme used in this chapter was Novozymes Cellic® CTec2 (lot# VCPI 0007), a blend of aggressive cellulases with high levels of β-glucosidases and hemicellulases that degrade lignocellulose into sugars (Novozymes, 2010). The protein concentration was determined to be 294 mg protein/mL with Pierce BCA assay (Zentay et al., 2016). Before use, the enzyme solution was diluted ten times with DI water.

Citrate Buffer

To maintain relatively high enzyme activity, citrate buffer (0.1-M) with a pH of 4.8 was used in enzymatic hydrolysis experiments. To prepare the buffer, citric acid monohydrate and trisodium citrate dihydrate were added to DI water.

Antibiotics

To prevent growth of contaminating microorganisms that could consume produced sugars, an antibiotic cocktail was added. To prepare the solutions, tetracycline powder was dissolved in an aqueous solution of 70% ethanol at 10 g/L and cycloheximide powder was dissolved in DI water at 10 g/L.

Enzymatic Hydrolysis

In the enzymatic hydrolysis experiments, desired amounts of α-cellulose, glucose, and DI water together with 125 mL citrate buffer, 2 mL tetracycline solution, and 1.5 mL cycloheximide solution were added to a 1-L centrifuge bottle in sequence and then preheated. When the mixture reached 50°C, enzymes were added. Then, the centrifuge bottle (total working volume of 250 mL) was placed in the incubator at 50°C for 10 days with an axial rotation of 2 rpm. Liquid samples of 0.5 mL were taken periodically and submerged in boiling water for 20 min to deactivate the enzymes. (*Note:* The volume of liquid sample is small relative to the total slurry volume, so it is assumed to have a negligible impact on substrate concentration.) Then, to determine the glucose concentration, the samples were filtered and analyzed by an HPLC, which was equipped with a pair of de-ashing guard columns (Bio-Rad Micro-Guard de-ashing

cartridges, 30 mm × 4.6 mm) and an HPLC carbohydrate analysis column (BioRad Aminex HPX-87P, 300 mm × 7.8 mm).

Selection of Hydrolysis Conditions

Experiments for Model Fitness

Based on our previous study (Zentay et al., 2016), 16 enzymatic hydrolysis conditions were tested including four different substrate concentrations (40, 60, 80, and 100 g/L), two different enzyme loadings (2 and 5 mg/g), and two different initial glucose concentrations (0 and 33 g/L).

Experiments for Model Predictions

Three enzymatic hydrolysis conditions – which were different from the conditions used for model fitness – were tested for model predictions: (1) substrate concentration: 40 g/L, enzyme loading: 1 mg/g, initial glucose concentration: 0 g/L; (2) substrate concentration: 70 g/L, enzyme loading: 1 mg/g, initial glucose concentration: 28 g/L; (3) substrate concentration: 100 g/L, enzyme loading: 5 mg/g, initial glucose concentration: 28 g/L.

Enzyme Stability

Enzyme stability was measured by quantifying the soluble protein concentration over the course of 20 days. In this experiment, the desired amount of CTec2 was added to the preheated mixture of citrate buffer, DI water, and antibiotic cocktail. The resulting solution was placed in the incubator at 50℃. Samples of 0.5 mL were taken periodically

and then centrifuged at 13,000 rpm for 10 min. The protein concentration of the supernatant was measured by the Pierce BCA method.

Modification of HCH-1 Model

Simulation of Enzyme Stability

Wallace *et al.* (2016) reported that unproductive binding with lignin and thermal deactivation may play a significant role in enzyme deactivation. Considering the substrate used in this chapter is lignin-free, we assume that enzyme deactivation is solely due to thermal deactivation. Rosales-Calderon *et al*. (2014) observed that the protein concentration of a mixture of glucanase and β-glucosidase dropped 34% after incubating at 50℃ for 4 days. It was hypothesized that the enzyme proteins suffered a structural change at 50℃, which led to protein aggregation and precipitation. Additives, whose concentration was assumed constant and proportional to the initial enzyme protein concentration, were supposed to be present in the cocktail to stabilize the enzyme protein against aggregation. Eq. 3-2 incorporates the presence of additives and is proposed to model protein stability (Rosales-Calderon *et al*., 2014). The development of Eq. 3-2 is described in detail by Rosales-Calderon *et al.* (2014).

$$-\frac{d[E]}{dt} = k_1[E] - k_2([E_0] - [E])[E_0] \qquad (3\text{-}2)$$

where,

E is the native enzyme protein concentration (g/L)

E_0 is the initial enzyme protein concentration (g/L)

k_1 and k_2 are the rate constants (h^{-1}).

The stability of CTec2 with three different initial concentrations was tested. Eq. 3-2 was used to fit the experimental data.

Modification of HCH-1 Model

The HCH-1 model was modified by the following steps:

Step 1: Use an empirical equation (Eq. 3-3) to fit the experimental data of the 16 enzymatic hydrolysis conditions (Section: Experiments for model fitness) with high accuracy. This smoothed version of the data provides the reaction rates needed to fit the parameters in the modified HCH-1 model of enzymatic hydrolysis.

$$\frac{d[G_1]}{dt} = \frac{3.7798([G_x^0]-[G_1])^{0.6410}\left(\frac{[E_0]\left(0.0574[E_0]+0.4370\exp\left(-t(0.4370+0.0574[E_0])\right)\right)}{0.4370+0.0574[E_0]}\right)^{0.8500}}{1+0.0247[G_1]^{1.1579}} \quad (3\text{-}3)$$

where,

G_x^0 is the initial cellulose concentration (g/L, equivalent to glucose).

Eq. 3-3 was developed based on the integrated version of Eq. 3-2 and an empirical model for batch fermentation (Fu and Holtzapple, 2010a). Detailed development of this equation is described in Appendix A. To fit the parameters, Eq. 3-3 was solved with the *ode45* routine in MATLAB and nonlinear optimization was achieved by the *fmincon* routine. The objective function was the sum of square errors (SSE), which is the sum of the squared difference between experimental data and the predicted value (Ordoñez et al., 2016). The optimal set of parameters corresponds to the smallest SSE value. This empirical correlation of the data provided a coefficient of determination R^2 = 0.994.

Step 2: Divide substrate conversion (from 0 to 1) into 50 equal segments. Using Eq. 3-3, calculate the reaction rate at each conversion and get a 16 × 50 dataset.

Step 3: Determine product inhibition.

The inhibition parameter *i* in the HCH-1 model was calculated by determining the initial velocities with and without inhibitor (Eq. 3-4) (Holtzapple et al., 1990). To estimate this value, the same enzyme and cellulose concentrations should be used.

$$i = \frac{V_{with\ inhibitor}}{V_{no\ inhibitor}} = \frac{\left[\frac{\kappa[G_x^0][E]}{\alpha + [G_x^0] + \varepsilon[E]}\right] i}{\frac{\kappa[G_x^0][E]}{\alpha + [G_x^0] + \varepsilon[E]}} \tag{3-4}$$

The inhibition of enzymatic hydrolysis by cellobiose was not considered in this study because CTec2 contains a high level of β-glucosidase that rapidly converts produced cellobiose into glucose; the cellobiose peak was not found in the HPLC results. For a single inhibitor, the inhibition parameter *i* is expressed in Eq. 3-5 and the glucose binding constant β_1 is calculated with Eq. 3-6.

$$i = \frac{1}{1 + \beta_1[G_1]} \tag{3-5}$$

$$\beta_1 = \frac{(1 - i)}{i[G_1]} \tag{3-6}$$

Step 4: Use the HCH-1 model to fit the 16 reaction conditions at each conversion, and determine the best-fit coefficients κ, α, and ε.

Step 5: Determine the relationship between parameter κ and conversion *x*.

Figure 3-2 presents the relationship between parameter κ in the HCH-1 model and substrate conversion *x*. The data were obtained from Steps 1−4. As shown in the

figure, κ drops very fast in the beginning and then stabilizes after conversion reaches 0.38. Nidetzky and Steiner (1993) assumed that cellulose consists of an easily hydrolyzable part and a recalcitrant part. Based on their two-substrate hypothesis, the authors derived a mathematical model to describe the kinetics of cellulose hydrolysis. According to the simulation results, the obtained rate constant for easily hydrolyzable cellulose was much higher than that of recalcitrant cellulose. Using α-cellulose as substrate, they determined that the fraction of easily hydrolyzable cellulose was 0.3 ((Nidetzky and Steiner, 1993). Figure 3-2 can be explained by this hypothesis, but the rate constant for the easily hydrolyzable cellulose decreases as conversion increases instead of being constant. In our experiments, the fraction of easily hydrolyzable cellulose (0.38) is close to the result in Nidetzky and Steiner (1993).

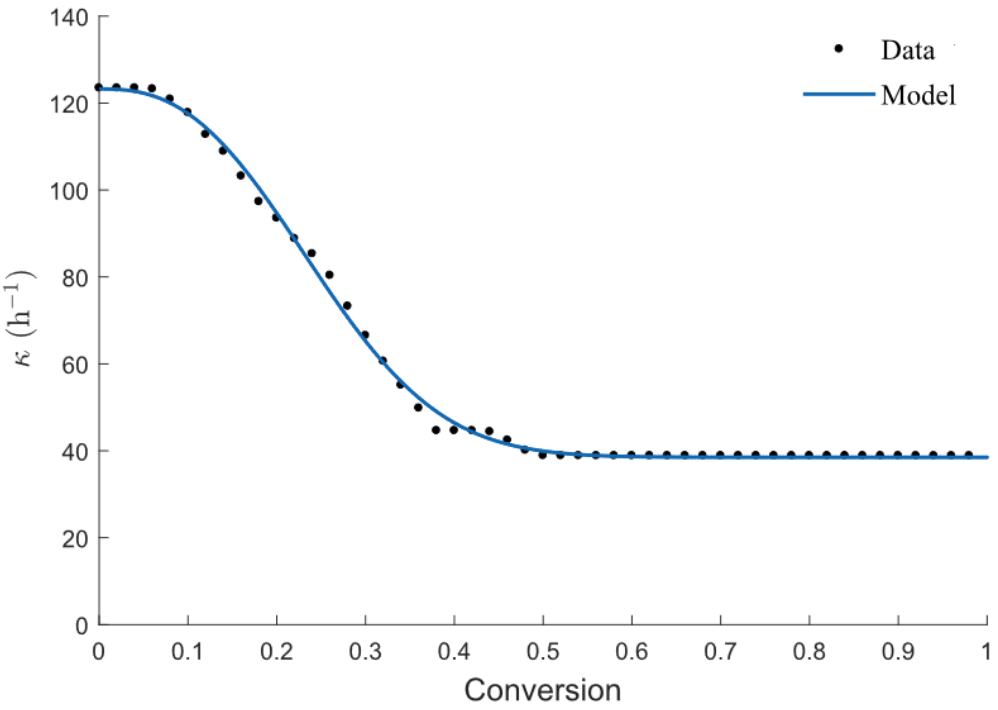

Figure 3-2 The relationship between parameter κ and conversion x.

Eq. 3-7 was developed to describe the relationship between parameter κ and conversion x.

$$\kappa = \frac{k_3}{(1 + x^{k_4})^{k_5}} + k_6 \tag{3-7}$$

where,

x is the substrate conversion

k_3, k_4, k_5, and k_6 are the parameters.

The conversion x in the denominator is used to describe the negative effect of conversion on the rate constant. The parameter k_6 is considered as the rate constant for recalcitrant cellulose. The parameter k_3 is used to describe the difference in rate

constants between the easily hydrolyzable cellulose (initial) and recalcitrant cellulose (height of the curve). The parameters k_4 and k_5 are used to describe the decrease rate of the rate constant (steepness of the curve) for the easily hydrolyzable part. To fit the data, the MATLAB curve fitting tool was used and a coefficient of determination $R^2 = 0.998$ was acquired. The values of parameters k_3, k_4, k_5, and k_6 were determined in this step.

Step 6: Determine the relationship between parameter ε and conversion x.

Figure 3-3 shows the relationship between parameter ε in the HCH-1 model and conversion x. As shown in the figure, parameter ε has a very narrow range (0–0.5) over the entire conversion and remains almost unchanged (nearly zero) at conversion 0.1−0.95. Therefore, in this study, parameter ε is assumed not to be affected by conversion and its optimal value should be close to zero. Brown and Holtzapple (1990) reported that if $[G_x^0]/[E_0] > 35$, assuming $\varepsilon = 0$ would not introduce considerable error (<1%). (*Note:* In our study, $[G_x^0]/[E_0] \geq 200$.) The parameter ε is needed only at high enzyme loadings. In industrial-scale saccharification, considering the high cost of enzymes, the enzyme dosage must be very low; therefore, if modeling a commercial process, the value of ε can be set as zero.

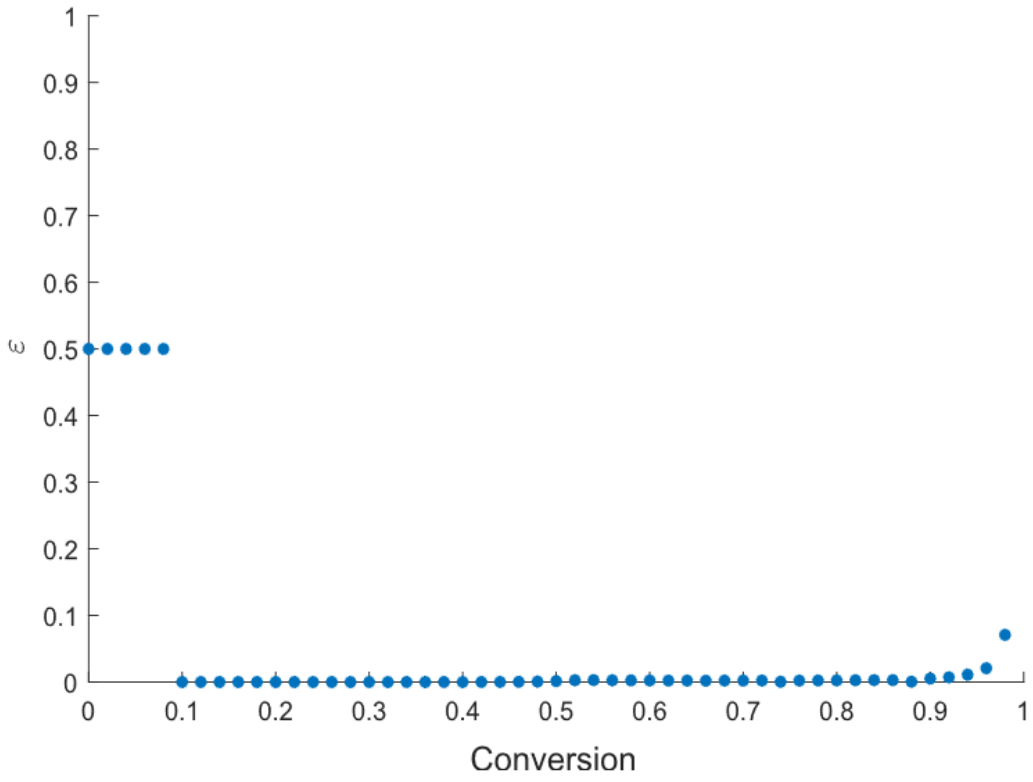

Figure 3-3 The relationship between parameter ε and conversion x.

Step 7: Determine the relationship between parameter α and conversion x.

The parameter α in the original HCH-1 model may be expressed by Eq. 3-8, which is related to enzyme adsorption.

$$\alpha = \frac{[E^f][G_x^f]}{[E^a] + [EG_x]} \tag{3-8}$$

Kumar and Wyman (2008) showed that glucose addition and enzyme dosage can affect the percentage of cellulase adsorption. Therefore, besides the impact of conversion, the effects of glucose and enzyme concentration on the value of α were tested. Using the best-fit coefficients κ and ε obtained from Step 4, two optimal α values

corresponding to two initial glucose concentrations were determined by fitting the data (eight data at each initial glucose concentration) from Step 2 at each conversion with the HCH-1 model (Figure 3-4a). Another two optimal α values corresponding to two enzyme concentrations were determined by repeating this procedure at each conversion (Figure 3-4b). As shown in Figure 3-4, as the reaction proceeds, the value of α increases and then is unchanged when the conversion reaches a certain point. It is obvious that high initial glucose concentration and low enzyme dosage improves the value of α significantly over the entire conversion range. Eq. 3-9 was proposed to describe the relationship among α, conversion x, enzyme concentration E, and glucose concentration G_1. As shown in Figure 3-4, all four curves show an "S" shape; therefore, the sigmoid function – which has an S-shaped curve – was used. The core structure of Eq. 3-9 is a sigmoidal function that describes the relationship between parameter α and conversion x. (*Note:* a_2 and a_3 are the parameters of the sigmoid function.) Also, because of the significant effect of glucose and enzyme concentrations on the value of α, the terms $[G_1]$ and $[E]$ were included in the numerator and denominator of the sigmoid function, respectively. The parameter a_1 was added to describe the weight of terms $[G_1]$ and $[E]$.

$$\alpha = \frac{a_1[G_1]}{[E](1 + \exp(-a_2 x + a_3))} \tag{3-9}$$

where,

a_1, a_2, and a_3 are the parameters.

Step 8: Modify HCH-1 model

Summarizing the proposed equations, Eq. 3-10 is the modified HCH-1 model, where k_1, k_2, k_3, k_4, k_5, k_6, a_1, a_2, a_3, ε, and β_1 are parameters. Estimates for k_1, k_2, k_3, k_4, k_5, k_6, and β_1 were determined in previous steps. In this step, the optimal values of a_1, a_2, a_3, and ε were determined by simultaneously fitting the experimental data of the 16 enzymatic hydrolysis conditions (Section: Experiments for model fitness) with Eq. 3-10.

$$\frac{d[G_1]}{dt} = \frac{\kappa[G_x][E]i}{\alpha + \varphi[G_x] + \varepsilon[E]}$$

where,

$$i = \frac{1}{1 + \beta_1[G_1]}$$

$$\varphi = \frac{[G_x] - \alpha - \varepsilon[E] + \sqrt{([G_x] - \alpha - \varepsilon[E])^2 + 4\alpha[G_x]}}{2[G_x]}$$

$$-\frac{d[E]}{dt} = k_1[E] - k_2([E_0] - [E])[E_0]$$

$$\kappa = \frac{k_3}{(1 + x^{k_4})^{k_5}} + k_6$$

$$\alpha = \frac{a_1[G_1]}{[E](1 + \exp(-a_2 x + a_3))} \qquad (3\text{-}10)$$

Integration of the differential equations described in Eq. 3-10 was performed using the same numerical methods described in Step 1.

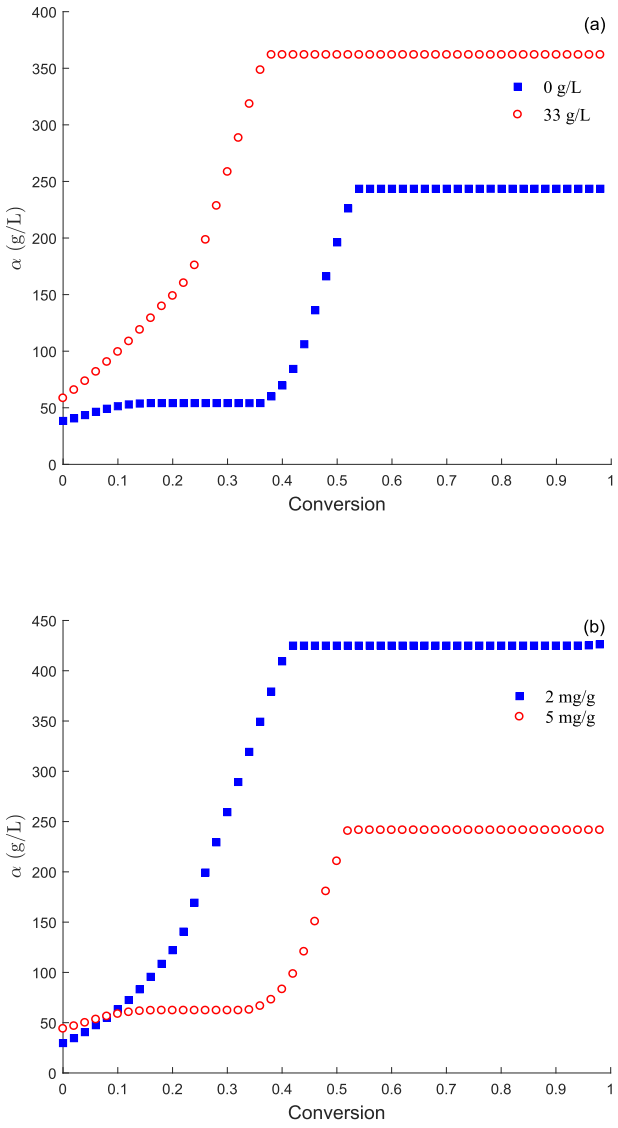

Figure 3-4 The relationship between parameter α and conversion x with (a) different initial glucose concentrations and (b) different enzyme loadings.

Sensitivity Analysis

Local Sensitivity Analysis

Local sensitivity analysis assesses the local impact of variation in input factors on model outputs. To do this analysis, the direct differential method (Peri et al., 2007) was used by calculating the sensitivity indices (Eq. 3-11). The sensitivities of parameters k_1, k_2, and β_1 were not analyzed because their values were obtained from independent experiment or calculation.

$$S_{p_j} = \frac{\partial y}{\partial p_j}\frac{p_j}{y} \tag{3-11}$$

where,

S_{p_j} is the non-dimensional sensitivity index of the j^{th} parameter

y is the glucose concentration (g/L)

p_j is the j^{th} parameter in the parameter vector p.

Global Sensitivity Analysis

Local sensitivity only analyzes the sensitivity of a solution close to the optimal parameter set. In contrast, global sensitivity analysis assesses the sensitivity of the model for the full range of possible parameter values (Ordoñez et al., 2016). Also, global sensitivity indices can evaluate the combined impact of multiple parameters on model output.

To calculate a global sensitivity index, a normally distributed search of parameter space using the Monte Carlo method was performed and subsequent analysis of the

variance in the model outputs was used. In this study, two global sensitivity indices were calculated: first-order index and total-effect index (Ordoñez et al., 2016; Sobol, 2001). The first-order index measures the effect of the parameter of interest alone on the output variance. The total-effect index accounts for not only the effect of the parameter of interest, but also interactions between other parameters and the parameter of interest at any order.

Model Evaluation

The modified HCH-1 model was compared with literature models for long-term enzymatic hydrolysis. As described in Step 1, the same differential equation integration method, nonlinear optimization constraint algorithm, and objective function were used. The Akaike information criterion (AIC) was used to evaluate model quality for the experimental data. The corrected version of AIC (AICc, Eq. 3-12) was used because the number of observations was not large enough.

$$AICc = N \cdot \ln\left(\frac{SSE}{N}\right) + 2(P+1) + 2\frac{(P+1)(P+2)}{N-P} \tag{3-12}$$

where,

N is the number of observations

P is the number of model parameters

SSE is the sum square error.

Results and Discussion

Enzyme Deactivation

Figure 3-5 shows that after incubating at 50℃ for 20 days, soluble protein concentrations of CTec2 dropped to 74%, 77%, and 83% of their initial values of 0.15, 0.26, and 0.61 g/L, respectively. This result is consistent with a previous study (Rosales-Calderon et al., 2014) that shows higher initial protein concentrations favor lower deactivation rates and supports the additive hypothesis. Eq. 3-2 successfully describes the time profiles of CTec2 protein concentration with a coefficient of determination R^2 = 0.999. The rate constants in Eq. 3-2 were determined to be k_1 = 0.0225 h^{-1} and k_2 = 0.1740 L/(g·h). It should be noted that the modified HCH-1 model is a "lumped" model, the performance of each enzyme was not modeled individually; therefore, the stability of each component in the enzyme cocktail was not investigated. Eq. 3-2 describes the overall deactivation of the cocktail.

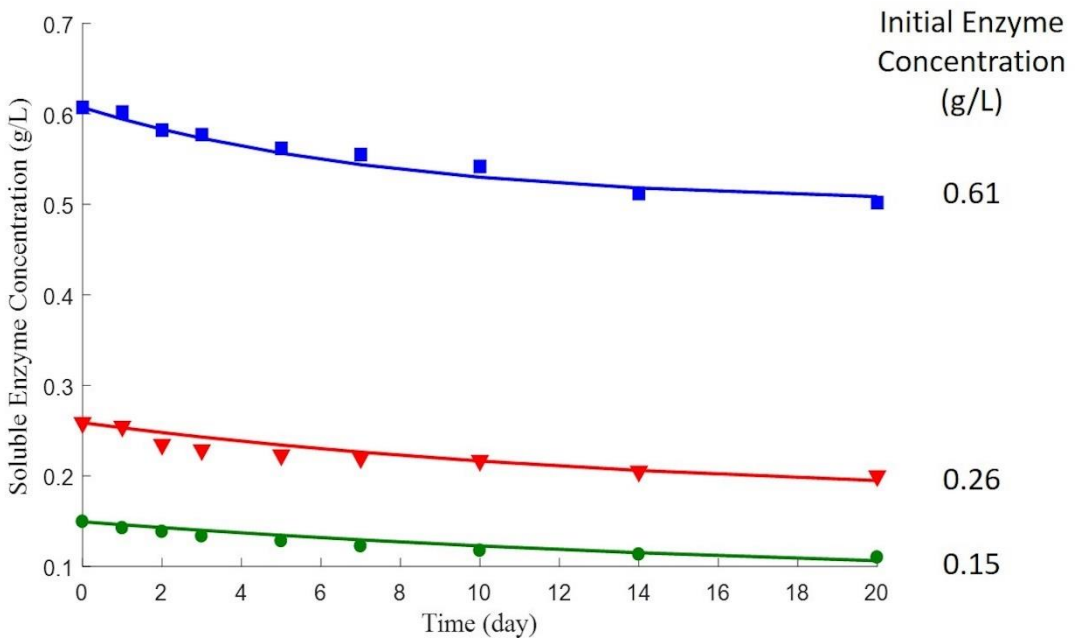

Figure 3-5 Time profiles and model predictions for soluble CTec2 protein concentration at 50°C. Experimental data are presented by the markers and the optimal fit by the solid lines.

Production Inhibition

Table 3-1 lists the values of glucose binding constant calculated from various reaction conditions. The eight β_1 values are very close to each other and have a standard deviation of 6×10^{-6} L/g. The mean value 0.0429 L/g is considered to be the "true" β_1 value and is used for later calculations.

Table 3-1 Glucose binding constant from various reaction conditions

Reaction condition		$\boldsymbol{\beta_1}$ **(L/g)**
Substrate concentration (g/L)	**Enzyme loading (mg/g)**	
40	2	0.042908
40	5	0.042915
60	2	0.042912
60	5	0.042918
80	2	0.042920
80	5	0.042923
100	2	0.042922
100	5	0.042925

Model Validation

Figure 3-6 shows the experimental data and modified HCH-1 model fitting results for enzymatic hydrolysis with 16 reaction conditions (Section: Experiments for model fitness). Table 3-2 shows the values of the parameters obtained from the previous section. The model simulation provided the coefficient of determination R^2 = 0.992, which indicates the modified HCH-1 model describes enzymatic hydrolysis of α-cellulose very well.

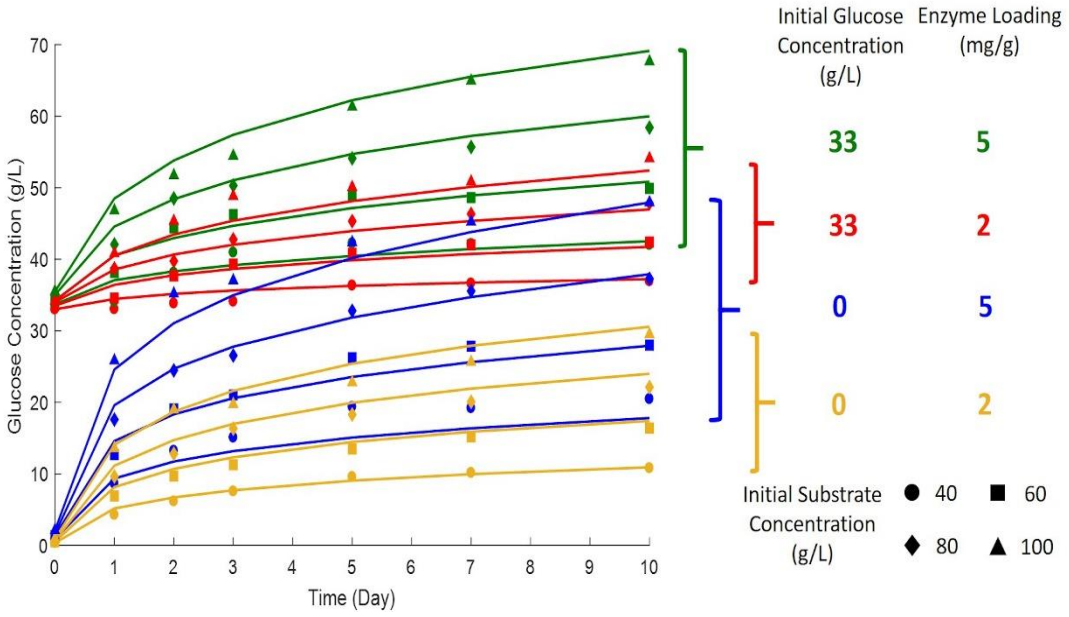

Figure 3-6 Time profiles and modified HCH-1 model fitting results for enzymatic hydrolysis of α-cellulose.

Table 3-2 Optimal parameter estimates for the modified HCH-1 model

Parameter	Value	Unit
k_1	0.0225	h^{-1}
k_2	0.1740	L/(g·h)
k_3	84.7500	h^{-1}
k_4	2.5800	dimensionless
k_5	26.3600	dimensionless
k_6	38.5000	h^{-1}
a_1	1.6791	g/L
a_2	31.1485	dimensionless
a_3	2.8452	dimensionless
ε	5.5248×10^{-5}	dimensionless
β_1	0.0429	L/g

As a comparison, Figure 3-7 shows the original HCH-1 model fit to the experimental data with 16 reaction conditions (Section: Experiments for model fitness). The value of β_1 (0.0429 L/g) was obtained from the previous section (Product inhibition). The optimal values (α = 2.0776 × 10^6 g/L, κ = 9.2889 × 10^5 h^{-1}, ε = 0.9996) were determined. (*Note:* Because the original HCH-1 model was not developed for integrated cellulose hydrolysis, these parameter values are not be meaningful.) The

model simulation provided the coefficient of determination R^2 = 0.947. The calculated SSE and AICc are listed in Table 3-3.

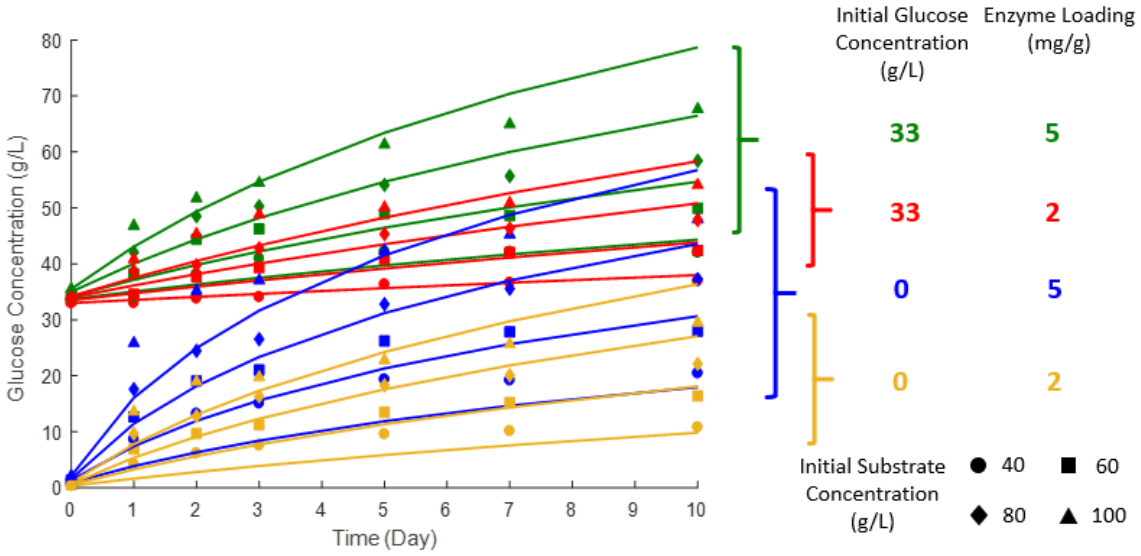

Figure 3-7 Time profiles and original HCH-1 model fitting results for enzymatic hydrolysis of α-cellulose.

Model Predictions

The modified HCH-1 model (Eq. 3-10) was used to predict the experimental results of the three conditions described in "Experiments for model prediction." The parameter values were obtained from the fitness of the 16 conditions (Table 3-2). The experimental and predicted results are shown in Figure 3-8. The simulation provided the coefficient of determination R^2 = 0.991, which indicates the modified HCH-1 model predicts enzymatic hydrolysis of α-cellulose with high accuracy.

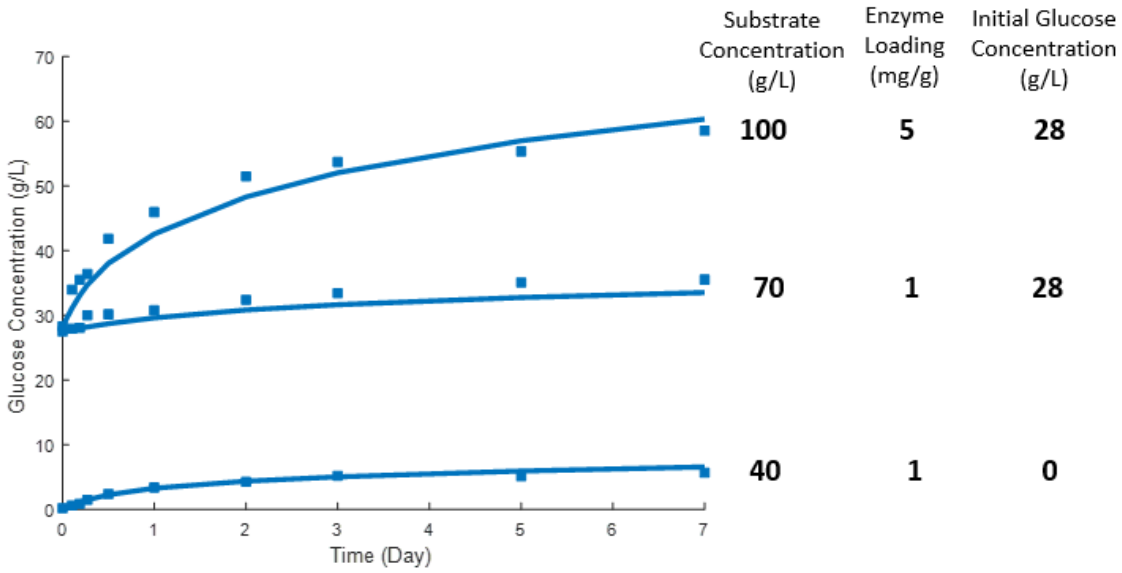

Figure 3-8 Time profiles and modified HCH-1 model predictions for enzymatic hydrolysis of α-cellulose. Experimental data are presented by the markers and the values of parameters are from Table 3-2.

Sensitivity Analysis

To explore the controlling factors in the proposed model at different hydrolysis stages, local and global sensitivity analyses were performed. Figure 3-9 shows the parameter sensitivity indices from local sensitivity analysis of the modified HCH-1 model over the course of 10 days. As shown in the figure, the sensitivity of k_3 drops to nearly 10% of its initial value at Day 10. The sensitivity of k_4 increases first and reaches up to 0.4 at around Day 1 and then slightly decreases from Day 2 to Day 10. For the parameters about α, the sensitivity of a_1 (absolute value) increases as the hydrolysis time increases. The sensitivities of a_2 and a_3 only change within the first several reaction

days, and then are close to zero after Day 3. The sensitivity of ε is close to zero during the entire reaction time.

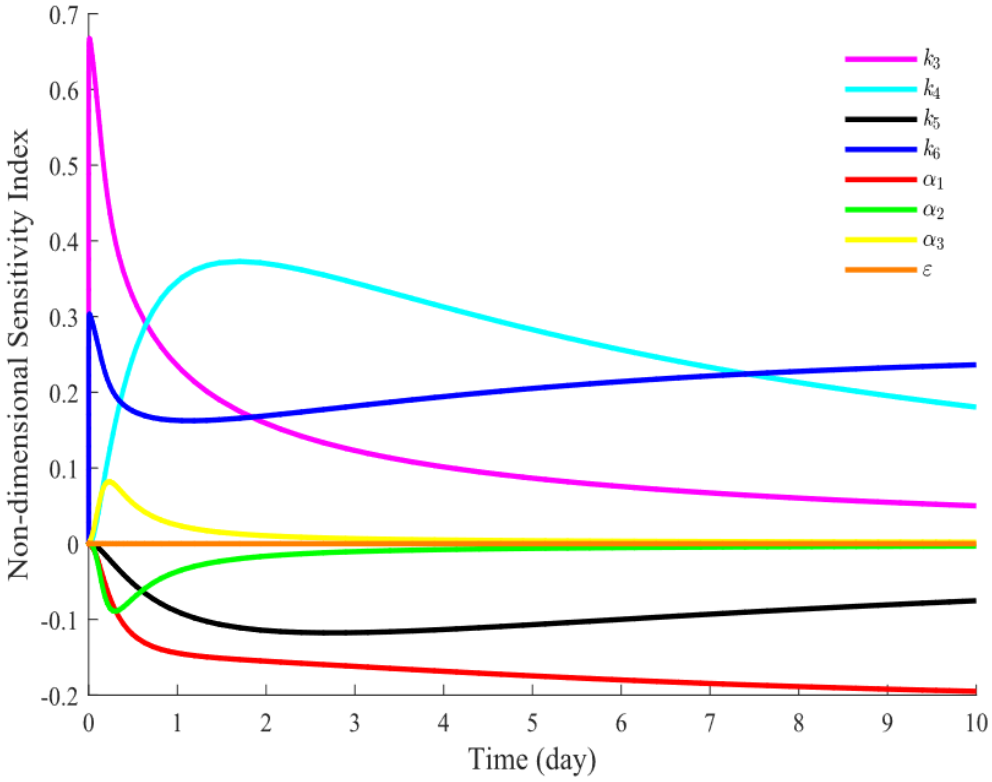

Figure 3-9 Local sensitivity analysis of the modified HCH-1 model at the optimal solution.

Figures 3-10a and 3-10b show the global sensitivity analysis results of the modified HCH-1 model. According to the figures, the first-order indices and total-effect indices of all variables are almost identical at any time, which means the variance in this model is not related to any interaction between parameters. At the initial stage of hydrolysis, the variance in the model output only depends on k_3 and k_6. Then, the

sensitivity index of k_3 decreases very fast during the first two days whereas k_4 increases up to 0.6. From Day 2 to Day 10, the effects of k_6 and a_1 on the model increase. The variables a_2, a_3, and ε do not show significant effects on the variance in model predictions.

According to Figures 3-9 and 3-10, the local and global sensitivity analyses of the modified HCH-1 model show a similar trend during the entire reaction time. Figure 3-11 shows the sensitivity indices calculated from both analyses at Day 10. The rankings of the eight sensitivity indices from both analyses are almost the same ($k_6 > a_1 > k_4 > k_5 > k_3 > a_2 \approx a_3 \approx \varepsilon$).

The sensitivity analyses not only determine which parameters have the most influence on model results, but also verify the assumption in Step 6 that the parameter ε is not needed at low enzyme loadings. These analyses provide direction for further modification of the HCH-1 model to apply it to real-world lignocellulose that contains lignin.

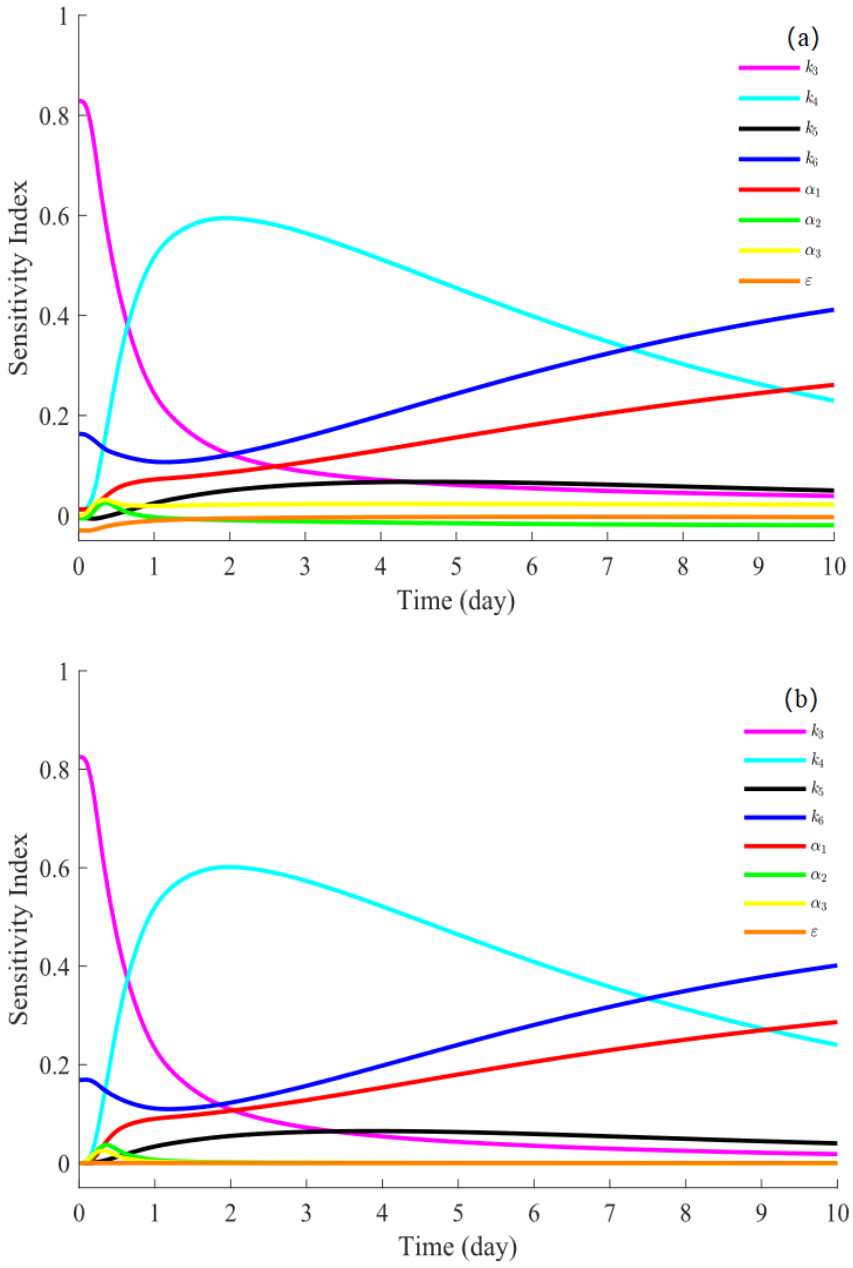

Figure 3-10 Global sensitivity analysis of the modified HCH-1 model over the course of 10 days, (a) first-order indices, (b) total-effect indices.

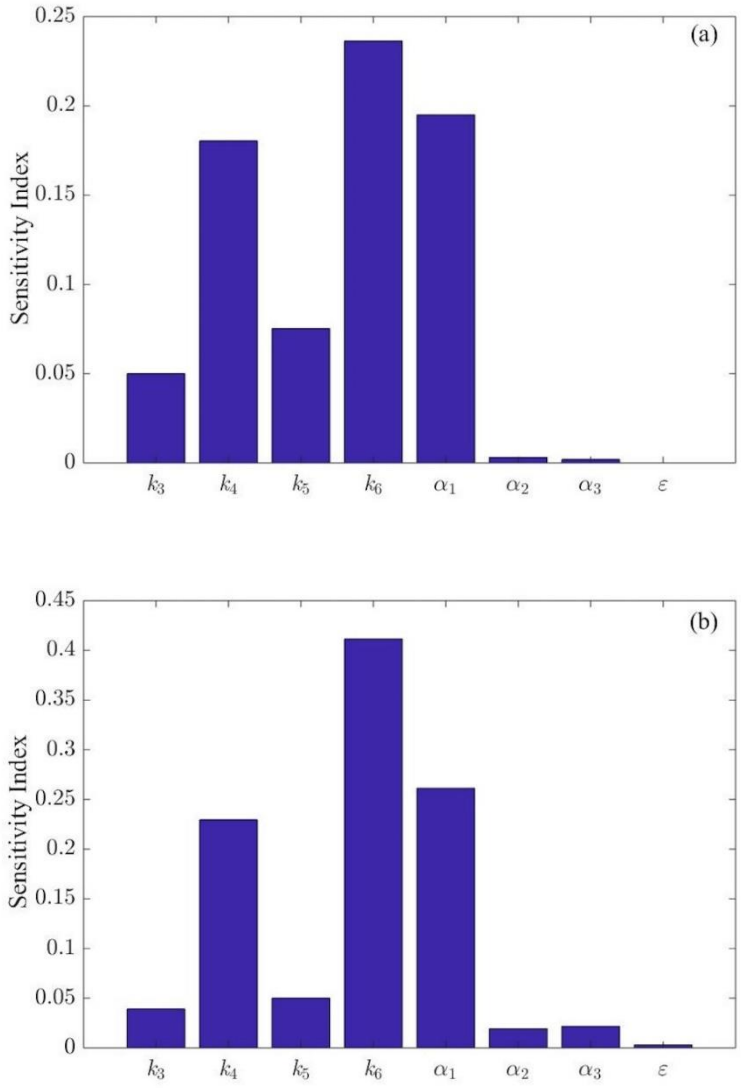

Figure 3-11 The local and global sensitivity indices of the modified HCH-1 model at Day 10. (a) local sensitivity analysis, (b) global sensitivity analysis (first-order indices).

Model Comparison

Based on the methodology used, published mechanistic and semi-mechanistic

models for cellulose and lignocellulose can be broadly divided into two classes: Michaelis–Menten and enzyme-adsorption models (Bansal et al., 2009). The models following Michaelis–Menten kinetics can also be divided into two subclasses: full Michaelis–Menten models (all rate equations follow Michaelis–Menten kinetics, including the steps of cellulose to cellobiose, cellulose to glucose, and cellobiose to glucose) and partial Michaelis–Menten models (only the step of cellobiose to glucose follows these kinetics). Models employing enzyme adsorption typically use Langmuir adsorption isotherms or the help of kinetic equations (Bansal et al., 2009). Some literature models incorporate both enzyme adsorption and Michaelis–Menten kinetics.

In this study, published models for long-term enzymatic hydrolysis of cellulose and lignocellulose were fit to the experimental data using the numerical methods described in Step 1. Some models do not consider product inhibition. To make a fair comparison, these models were only fit to experimental conditions with no initial sugar added (0 g/L initial glucose, four substrate concentrations × two enzyme loadings). Some models teased out fine details in the elementary reaction steps and included some variables that were not determined in this study, such as exocellulase concentration and associated enzyme concentration (Shang et al., 2013; Cruys-Bagger et al., 2016; Jeoh et al., 2017). These models are not included in this section. Table 3-3 summarizes the number of observations and parameters, calculated SSE and AICc values, and the methodology used for the published models. According to the table, the modified HCH-1 model has the least SSE and AICc values, which indicates this model provides the best fit for long-term enzymatic hydrolysis of α-cellulose.

Table 3-3 Comparison of long-term enzymatic hydrolysis models

Model	N (Obs)	Parameter	SSE	AICc	Methodology
Modified HCH-1 (16)	112	11	236.7	110.9	Ads
Holtzapple *et al.* (1984) (original HCH-1)	112	4	1630.7	310.5	Ads
Drissen *et al.* (2007)	112	11	600.8	215.2	Ads, M–M
Fan and Lee (1983)	112	11	679.7	229.0	Ads
Liao *et al.* (2008)	112	5	1313.7	288.5	Ads
Peri *et al.* (2007)	112	12	2657.6	384.3	Ads, M–M
Fenila and Shastri (2016)	112	22	2080.9	385.5	Ads, M–M
Kadam *et al.* (2004)	112	18	2338.6	386.4	Ads, M–M
Gusakov *et al.* (1985)	112	16	2879.2	404.0	M–M
Philippidis *et al.* (1993)	112	7	9139.8	510.4	Ads, M–M
Modified HCH-1 (8)[a]	56	11	115.2	71.3	Ads
Shen and Agblevor[a] (2008)	56	4	493.8	133.1	Ads
Zhang *et al.*[a] (2010)	56	3	692.6	149.6	Ads
Rosales-Calderon *et al.*[a] (2016)	56	3	692.6	149.6	Ads
Nidetzky and Steiner[a] (1994)	56	5	743.9	158.5	Ads

M–M: Michaelis–Menten kinetics, Ads: Adsorption-based approach.

[a] Only eight reaction conditions were fit (0 g/L initial glucose, four substrate concentrations (40, 60, 80, and 100 g/L) × two enzyme loadings (2 and 5 mg/g)).

Conclusions

The original HCH-1 model was modified to extend its application to integrated enzymatic hydrolysis; it performed well when fitting 10-day cellulose hydrolysis at various experimental conditions. Local and global sensitivity analyses were performed to determine the controlling parameters at different hydrolysis stages. Mechanistic (and semi-mechanistic) literature models for long-term enzymatic hydrolysis were compared with the modified HCH-1 model and evaluated by AICc. Comparison results show that the modified HCH-1 model provides the best description of enzymatic cellulose hydrolysis. The "lumped" modified HCH-1 model developed in this study has a simpler form and fewer parameters than mechanistic models of each enzyme component. When each enzyme is modeled separately, the kinetics are extremely complex with the potential to over-parameterize. For the specific commercial enzyme cocktail used in this study, excellent fits to the data were obtained without the need to model each enzyme component individually.

CHAPTER IV

KINETIC MODELING OF COUNTERCURRENT SACCHARIFICATION[2]

Introduction

As shown in Chapter II, compared to traditional batch saccharification, countercurrent saccharification more fully utilizes enzymes and therefore reduces the enzyme loadings and lowers the cost of sugar and biofuel production. However, in countercurrent saccharification experiments, 3 to 4 months are usually required to acquire a single steady-state data point. To save time and labor, simulation of this process is necessary to test various reaction conditions and determine the optimal operating point. Previously, a suitable kinetic model for countercurrent saccharification has never been reported.

Loescher (1996) developed Continuum Particle Distribution Modeling (CPDM) theory and derived it for various reactor configurations (batch, fed batch, continuous stirred tank reactor (CSTR), plug flow reactor (PFR), countercurrent and cocurrent CSTR cascades, PFR-CSTR cascades, and CSTR-PFR cascades). Previous studies (Loescher, 1996; Ross, 1998; Thanakoses, et al., 2003; Fu and Holtzapple, 2010b; Darvekar and Holtzapple, 2016) showed that the CPDM model satisfactorily predicts countercurrent fermentation using mixed microbial cultures that digest various

[2] The content of this chapter is from: Liang, C., Gu, C., Karim, M.N., Holtzapple, M., 2019. Kinetic modeling of countercurrent saccharification. Biotechnology for Biofuels. 12: 179.

feedstocks. Here, CPDM is applied to countercurrent enzymatic saccharification of lignocellulose.

In this study, the CPDM model was used to simulate multi-stage countercurrent saccharification. α-Cellulose was used for modeling because of its simpler composition compared to real-world lignocellulose, which contains lignin. Lignin is known to bind cellulase enzymes non-productively (Kumar and Wyman, 2009b), which complicates the kinetic modeling. The predicted glucose concentrations and conversions were compared with experimental data and the average errors were calculated. In addition, the model estimated the effects of enzyme-addition location, total stage number, enzyme loading, liquid residence time (LRT), and solids loading rate (SLR) on conversion and product concentration, thus allowing the benefits of countercurrent saccharification over batch to be quantified.

Materials and Methods

Materials

In this chapter, the substrate used for all experiments was α-cellulose (Sigma Aldrich, C8002-5KG). Compositional analysis showed that the substrate contained glucan 78.5% and xylan 14.4% (Zentay et al., 2016). The enzyme used for all experiments was Novozymes Ctec2 (lot # VCPI 0007), a blend of aggressive cellulases with high levels of β-glucosidases and hemicellulases (Zentay et al., 2016; Lonkar et al., 2017). The protein concentration of the enzyme solution was determined to be 294 mg protein/mL with Pierce BCA assay (Zentay et al., 2016). To maintain relatively high enzyme activity, citrate buffer (0.1 M, pH 4.8) was used in all experiments in this

chapter. To prevent microbial growth, an antibiotic cocktail (tetracycline 10 g/L 70% ethanol and cycloheximide 10 g/L DI water) was used in all experiments in this chapter.

Countercurrent Saccharification

Experimental data of countercurrent saccharification were obtained from Zentay *et al*. (2016). In the experiments, two trains were performed with enzyme loadings of 2 and 5 mg/g, respectively (Trains 1 and 2 in Chapter II). Details of the experiments are shown in Chapter II and Table 2-1.

Continuum Particle Distribution Model

In CPDM, a "continuum particle" is defined as one gram of solids in the initial unreacted state and is representative of the substrate (Loescher, 1996; Ross, 1998; Darvekar and Holtzapple, 2016). This model tracks the reaction progress of the continuum particle as it transfers through the stage, digests, and releases products (Fu and Holtzapple, 2010c). Conversion of the particle from 0 to 1 is divided into a given number of intervals. A conversion distribution function (implicitly defined by Eq. 4-1) is used to express the number of continuum particles in each specific conversion interval at a particular reaction time.

$$n_0 = \int_0^1 \hat{n}(x)\, dx \tag{4-1}$$

where,

$\hat{n}(x)$ is the particle conversion distribution function

n_0 is the initial particle concentration (particle/L).

Eq. 4-2 relates the total reaction rate (r_t) with the reaction rate at a given conversion (r) as a function of particle conversion (x), product concentration (G_1), enzyme concentration (E), and particle conversion distribution $\hat{n}(x)$, which contains information about substrate concentrations (G_x) and conversions (x). (*Note:* The CPDM model was previously used to simulate countercurrent fermentation only. The governing rate equation used in the CPDM model was for batch fermentation. To simulate countercurrent saccharification, in this study, the governing rate equation of the CPDM model was changed.)

$$r_t = \int_0^1 r(\hat{n}(x), x, [G_1], [E])dx \tag{4-2}$$

where,

r_t is the total reaction rate (g/(L·d))

r is the reaction rate at a given conversion (g/(L·d))

G_1 is the glucose concentration (g/L)

E is the (native) enzyme concentration (g/L)

x is the substrate conversion (0 to 1)

To get a satisfactory prediction, the governing rate equation ($r(\hat{n}(x), x, [G_1], [E]]$) employed in the CPDM model should accurately describe batch enzymatic hydrolysis under various reaction conditions. The HCH-1 model, proposed by Holtzapple *et al*. (1984), is a generalized mechanistic model for cellulose hydrolysis. Compared to the classic Michaelis–Menten model, the HCH-1 model includes non-competitive inhibition and an added parameter ε that describes the number of reactive

sites covered by the enzymes (Holtzapple et al., 1984; Brown et al., 2010). Previous studies (Brown et al., 2010) showed that the HCH-1 model could predict short-term (initial-rate) enzymatic hydrolysis with high accuracy and better than other models that appeared in the literature. Chapter III modified the HCH-1 model to extend its application to long-term (>48 h) batch enzymatic hydrolysis. Comparison of mechanistic models under various reaction conditions showed that the modified HCH-1 model provided the best fit to experimental data of enzymatic hydrolysis of α-cellulose (Brown et al., 2010; Liang et al., 2019a; Chapter III). Therefore, the modified HCH-1 model (Eq. 3-10, parameter values from Table 3-2) was used as the governing rate equation in the CPDM model.

In the simulation of countercurrent saccharification, all stages were set to have the same initial conditions identical to the experiments. Combining Eq. 3-10 and Eq. 4-1, the reaction rate *r* of each conversion interval was calculated. Using Eq. 4-2, the total reaction rate r_t of each stage was calculated and the glucose concentration of each stage after 48-h reaction was obtained. Accordingly, the conversions of the continuum particles were changed from the previous conversion intervals to the higher intervals. Then, just like the experiments, a 1-mL liquid sample was taken from each stage; specific amounts of solids and liquid phases were transferred between stages; solids and liquids were removed from the last and first stages, respectively; and fresh solids, liquid, and enzymes were added to the system. The conversion distribution of continuum particles and glucose concentration of each stage were further changed based on the

transfer. Afterwards, the next 48-h reaction started. The previous steps were repeated until the total reaction time was reached.

Enzyme Stability

The operating time of the countercurrent experiments was usually longer than one month. To improve the countercurrent saccharification model, it is necessary to determine enzyme stability over a relatively long time. Rosales-Calderon *et al*. (2014) showed that the soluble protein concentration of a mixture of glucanase and β-glucosidase dropped significantly after incubating at 50℃ for 4 days and hypothesized that the enzyme proteins suffered a structural change, which led to protein aggregation and precipitation. Based on this hypothesis, Chapter III measured the stability of CTec2 by quantifying soluble protein concentration over the course of 20 days. Results showed that soluble CTec2 protein concentration dropped up to 26% after 20-day incubation at 50℃. Eq. 4-3 (proposed by Rosales-Calderon *et al*. (2014), parameter values from Chapter III) was used to model the stability of CTec2 successfully. To predict active enzyme concentration in the countercurrent process accurately, Eq. 4-3 was incorporated into the simulation of countercurrent saccharification. It should be noted that in batch simulation, Eq. 4-3 was part of the modified HCH-1 model. Here, it is incorporated into the CPDM model independently instead of being included in the governing equation because the addition locations of substrate and enzymes were different in the countercurrent system.

$$-\frac{d[E]}{dt} = 0.023[E] - 0.174([E_0] - [E])[E_0] \quad (4\text{-}3)$$

Enzyme Distribution

In every transfer of the countercurrent experiment, solid and liquid phases were separated by a centrifuge and transferred in the opposite direction. As the liquid/solid phases moved, the enzymes suspended in the liquid phase or absorbed on the solid phase would move with them. To predict accurately the enzyme concentration of each stage after every transfer, it is important to determine the distribution of enzymes between the two phases. Kumar and Wyman (2008) showed that glucose addition and enzyme dosage can affect the fraction of cellulase adsorption. In this study, glucose concentrations ranging from 0 to 93.35 g/L and enzyme loadings ranging from 1 to 5 mg/g were tested.

In the enzyme distribution experiments, the desired amounts of glucose, enzyme solution, and DI water together with 25 g α-cellulose, 125 mL citrate buffer, and 3.5 mL antibiotic solutions were added to a 1-L centrifuge bottle (total 250 g). Control experiments were also performed, which had the same loadings, but without substrate. To avoid hydrolysis, the loaded bottles were placed in the refrigerator (4°C). After equilibration overnight, the bottles were centrifuged to separate solid and liquid phases. The protein concentrations of supernatants were measured by the Bradford protein assay and the glucose concentrations of supernatants were analyzed by an HPLC that was equipped with a refractive index detector, autosampler, a pair of de-ashing guard columns (Bio-Rad Micro-Guard de-ashing cartridges, 30 mm × 4.6 mm), and an HPLC carbohydrate analysis column (BioRad Aminex HPX-87P, 300 mm × 7.8 mm). The fraction of enzyme absorbed on the solid phase was expressed by Eq. 4-4.

$$\text{Enzyme absorbed (fraction)} = 1 - \frac{\text{protein concentration of supernatant in test experiment}}{\text{protein concentration of supernatant in corresponding control experiment}} \quad (4\text{-}4)$$

Reactor Volume Calculation

The volume of the batch reactor was determined as follows:

$$\text{Batch reactor volume (L)} = \frac{\text{Glucose production rate } \left(\frac{\text{g glucose}}{\text{day}}\right) \times \text{ Batch residence time (day)}}{\text{Product concentration } \left(\frac{\text{g glucose}}{\text{L solution}}\right) \times \text{ Ratio A } \left(\frac{\text{L solution}}{\text{L slurry}}\right)} \quad (4\text{-}5)$$

where Ratio A is the volume of sugar solution per the measured volume of the slurry before reaction. For example, if the glucose concentration of the product is 100 g/L, the density of the solution is approximately 1040 g/L solution (The Engineering Toolbox, 2019). In 1 L of sugar solution, there are 100 g of glucose and 940 g water. To make that amount of glucose requires 90 g cellulose and 10 g of water; therefore, the slurry would be composed of 90 g cellulose and 950 g water. Assuming the density of solid is 1 g/mL, then Ratio A is 0.962.

The volume of the countercurrent reactor was determined as follows:

$$\text{Countercurrent reactor volume (L)}$$

$$= \text{Glucose production rate}\left(\frac{\text{g glucose}}{\text{day}}\right) \times \text{Ratio B}\left(\frac{\text{g water}}{\text{g glucose}}\right)$$

$$\times \text{Water density}\left(\frac{\text{L water}}{1000\ \text{g water}}\right) \times \text{Ratio C}\left(\frac{\text{L slurry}}{\text{L water}}\right)$$

$$\times \text{Liquid residence time (day)} \qquad (4\text{-}6)$$

where Ratio B is the ratio of the water mass to glucose mass at a specific glucose concentration, and Ratio C is the ratio of the initial total working volume to the loaded liquid volume. For example, if the solid concentration in the reactor is 250 g solids/L liquid, then Ratio C is the volume of 250 g solids + 1000 g water divided by the volume of 1000 g water. Assuming the density of solid is 1 g/mL, then Ratio C is 1.25.

In this study, to achieve a fair comparison, the batch reactor volume was considered identical to the continuous plug-flow reactor volume.

$$\frac{\text{Glucose production rate}\left(\frac{\text{g glucose}}{\text{day}}\right) \times \text{Batch residence time (day)}}{\text{Product concentration}\left(\frac{\text{g glucose}}{\text{L solution}}\right) \times \text{Ratio A}\left(\frac{\text{L solution}}{\text{L slurry}}\right)}$$

$$= \text{Glucose production rate}\left(\frac{\text{g glucose}}{\text{day}}\right) \times \text{Ratio B}\left(\frac{\text{g water}}{\text{g glucose}}\right)$$

$$\times \text{Water density}\left(\frac{\text{L water}}{1000\ \text{g water}}\right) \times \text{Ratio C}\left(\frac{\text{L slurry}}{\text{L water}}\right)$$

$$\times \text{Liquid residence time (day)} \qquad (4\text{-}7)$$

The glucose production rates of batch and countercurrent saccharifications were set equal, then,

$$\text{Liquid residence time (day)} = \frac{\text{Batch residence time (day)}}{\text{Product concentration}\left(\frac{\text{g glucose}}{\text{L solution}}\right) \times \text{Ratio A}\left(\frac{\text{L solution}}{\text{L slurry}}\right) \times \text{Ratio B}\left(\frac{\text{g water}}{\text{g glucose}}\right) \times \text{Water density}\left(\frac{\text{L water}}{1000\ \text{g water}}\right) \times \text{Ratio C}\left(\frac{\text{L slurry}}{\text{L water}}\right)} \quad (4\text{-}8)$$

The denominator has typical values of 1 to 1.25.

Eq. 4-8 specifies the required LRT for the countercurrent system that has the same volumetric productivity (g glucose/(L reactor·day)) as the batch reactor. Using this approach, the amount of enzyme required by each system can be compared on an equal and fair basis.

Results and Discussion

Enzyme Distribution

Figure 4-1 shows the effects of glucose and enzyme concentrations on the fraction of enzyme absorbed. As shown in this figure, additional glucose negatively affects enzyme absorption, which is consistent with the literature (Kumar and Wyman, 2008). As glucose concentration increases, more enzyme combines with glucose in the liquid, thus reducing the enzyme absorbed onto the solid phase. Also, as expected, higher enzyme loadings favor lower fractions of absorption because high dosage might saturate the adsorption of enzymes on the cellulose surface.

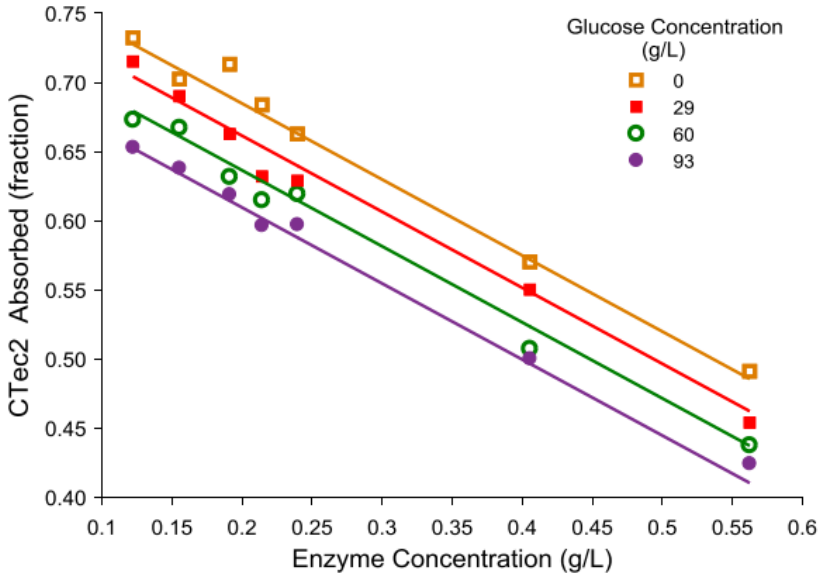

Figure 4-1 Effects of glucose and enzyme concentrations on the fraction of enzyme absorbed and fitted with Eq. 4-9. Experimental data are presented by the markers and the optimal fit by the solid lines.

To describe the experimental data, a linear equation (Eq. 4-9) was proposed and resulted in a high coefficient of determination (R^2 = 0.99). This equation was incorporated into the simulation of countercurrent saccharification to quantitatively determine the amount of enzymes in liquid and solid phases, thereby acquiring the transfer amounts and directions of enzymes.

$$y = d_1[E] + d_2[G_1] + d_3 \tag{4-9}$$

where,

y is the fraction of CTec2 absorbed

d_1, d_2, and d_3 are the parameters ($d_1 = -0.550$ L/g; $d_2 = -8.04\times10^{-4}$ L/g; $d_3 = 0.795$).

Verification of the CPDM Model

Figure 4-2 shows the predicted glucose concentrations as a function of time and stage number at enzyme loading of 5 mg/g. The predicted and experimental results (Figure 2-2) show similar trends. At the beginning, the glucose concentration significantly changes until it eventually stabilizes when the system reaches steady state. At steady state, the glucose concentration increases gradually from Stage 8 to Stage 1. Table 4-1 compares the experimental glucose concentrations (Stage 1) and conversions to the CPDM predictions at enzyme loadings of 2 and 5 mg/g. To be consistent with experiments, the operation time of the two trains in the simulation was set to be 24 and 42 days, respectively, when the systems have been verified to reach steady state in the experiments. According to Table 4-1, the CPDM predictions agree well with glucose concentrations from countercurrent experiments with an average error of 3.5%. The average error between experimental and predicted conversions is 4.7%.

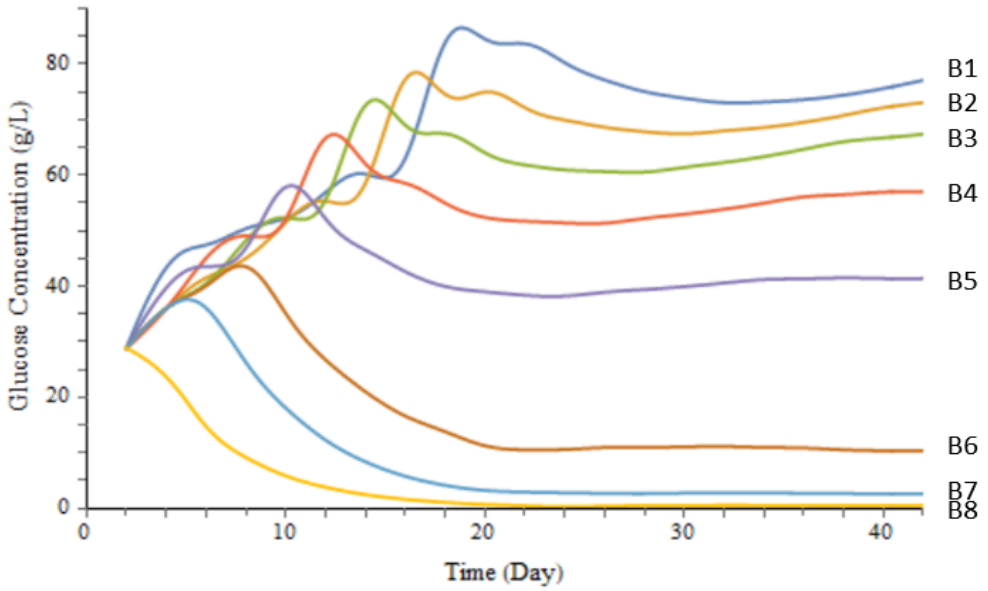

Figure 4-2 Predicted glucose concentration as a function of time and stage (bottle) number. Operation conditions in the simulation are set to be the same as the experimental conditions (listed in Table 2-1, Train 2).

Table 4-1 Comparison of experimental and predicted glucose concentrations and conversions for countercurrent saccharification of α-cellulose

Train	**1**	**2**	**Average**
Enzyme loading (mg/g)	2	5	
Glucose concentration (g/L)			
Experimental[1]	54	78	
Predicted from CPDM	51	77	
Error (%)[2]	5.6	1.3	3.5
Conversion (%)			
Experimental[1]	56	88	
Predicted from CPDM	52	86	
Error (%)[2]	7.1	2.3	4.7

[1] Data obtained from Zentay *et al*., 2016.

[2] Error (%) = |Predicted – Experimental|/Experimental × 100%.

Sensitivity Analysis

To explore the controlling parameters in the proposed model, sensitivity analyses were performed. Chapter III showed that k_3, k_4, k_6, and α_1 had the most influence on the modified HCH-1 model results. Therefore, the sensitivities of the four parameters

together with the three parameters d_1, d_2, and d_3 in the enzyme distribution equation (Eq. 4-9) were analyzed in this section (Figure 4-3).

As shown in Figure 4-3, in the space of 75–125% of parameter values, α_1 and d_3 –which are both related to enzyme adsorption – have the most influence on conversion. Among the parameters related to kinetics, k_6 – which is considered as the rate constant for recalcitrant cellulose (Chapter III) – has the most influence on conversion. The parameter d_2 – which weighs the effect of glucose concentration on the fraction of enzyme adsorbed – has the least influence on simulation results. These analyses provide insights to directions that would further optimize the countercurrent system.

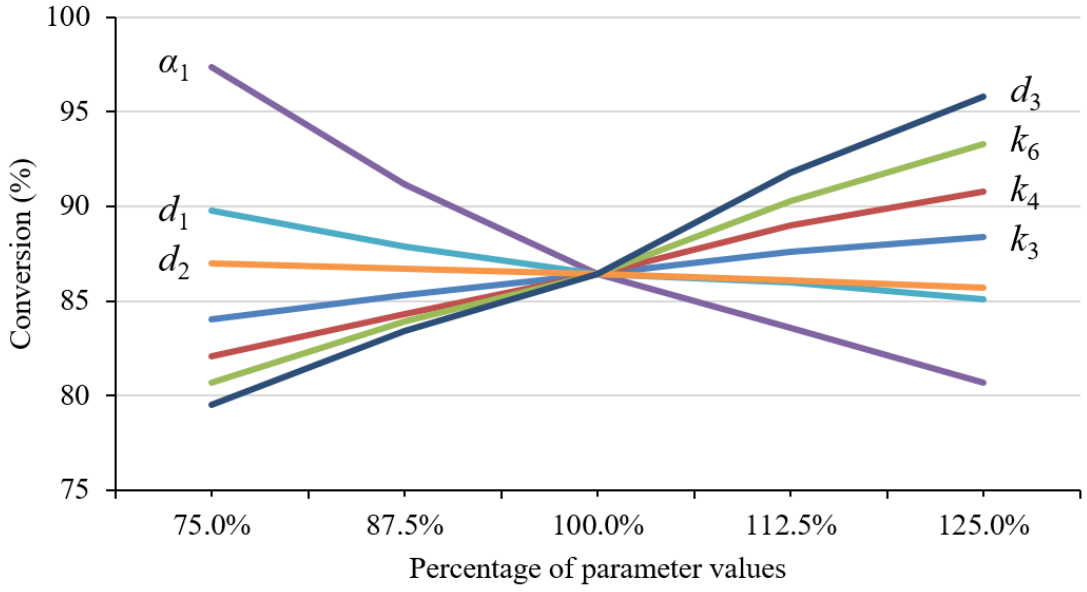

Figure 4-3 Sensitivity analysis of countercurrent saccharification simulation. Operation conditions in the simulation are set to be the same as the experimental conditions (listed in Table 2-1, Train 2).

Predictions from the CPDM Model

According to the verification results, CPDM is sufficiently accurate to determine the optimal operating conditions in countercurrent saccharification. In this section, CPDM was used to test the effects of enzyme-addition location, total stage number, enzyme loading, LRT, and SLR on conversion and product concentration. To ensure the simulated countercurrent systems reach steady state, the operation time of all simulations was set to 200 days.

Effect of Enzyme-addition Location

Determining the optimal enzyme-addition location maximizes the retention time of enzymes in the system and therefore fully uses substrate and enzymes. In this simulation study, various enzyme-addition locations were tested in the eight-stage countercurrent system at enzyme loadings of 2 and 5 mg/g (Figure 4-4). According to Figure 4-4, for both tested enzyme loadings, conversions increase as the enzyme-addition location moves from "front" to "back" of the system. For enzyme loading of 2 mg/g, the highest conversion is obtained when adding enzymes to Stage 7. For enzyme loading of 5 mg/g, the optimal addition location is Stage 8. Compared to low enzyme dosages, at high enzyme dosages, adding enzymes to the downstream brings more benefits. For example, at 2 mg/g, $\text{Conversion}_{\text{Stage 7}} - \text{Conversion}_{\text{Stage 1}} = 16\%$. In contrast, at 5 mg/g, $\text{Conversion}_{\text{Stage 8}} - \text{Conversion}_{\text{Stage 1}} = 45\%$. At high enzyme dosages, a larger proportion of enzymes are in the liquid phase (Section: Enzyme distribution between solid and liquid phases); therefore, adding enzymes near the "back" of the system increases enzyme retention.

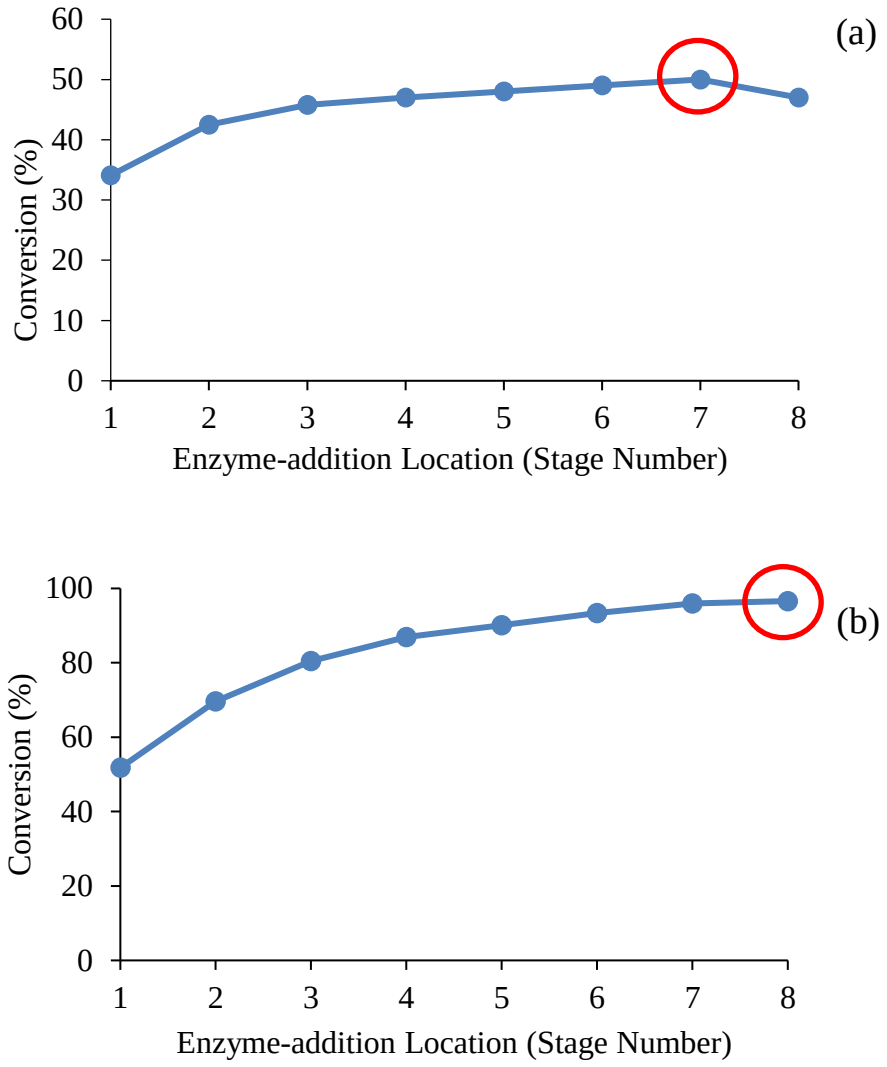

Figure 4-4 Effect of enzyme-addition location on conversion in the eight-stage countercurrent system at enzyme loadings of (a) 2 mg/g and (b) 5 mg/g using α-cellulose as substrate. Operation time is 200 days. Other conditions in this simulation are set to be the same as the experimental conditions. Simulation

data are presented by the markers and the lines are added to show the changing trend.

Effect of Total Stage Number

Figure 4-5 shows the effect of total stage number on conversion at enzyme loadings of 2 and 5 mg/g. In this simulation study, the transfer frequency was adjusted to ensure the LRTs of all tested conditions were the same (29 days). The enzyme-addition locations were set to the penultimate stage for enzyme loading of 2 mg/g (Figure 4-5(a)) and the last stage for enzyme loading of 5 mg/g (Figure 4-5(b)) (Section: Effect of enzyme-addition location). According to Figure 4-5, the optimal total stage number is affected by enzyme loading. For enzyme loading of 2 mg/g, the highest conversion is obtained with a 16-stage system. For enzyme loading of 5 mg/g, the highest conversion is obtained with a four-stage system. This result indicates that for the same LRT, a higher-stage system is more beneficial when the enzyme loading is low. In the later simulations, various enzyme loadings were used; therefore, to make a fair comparison, a constant eight-stage system was used.

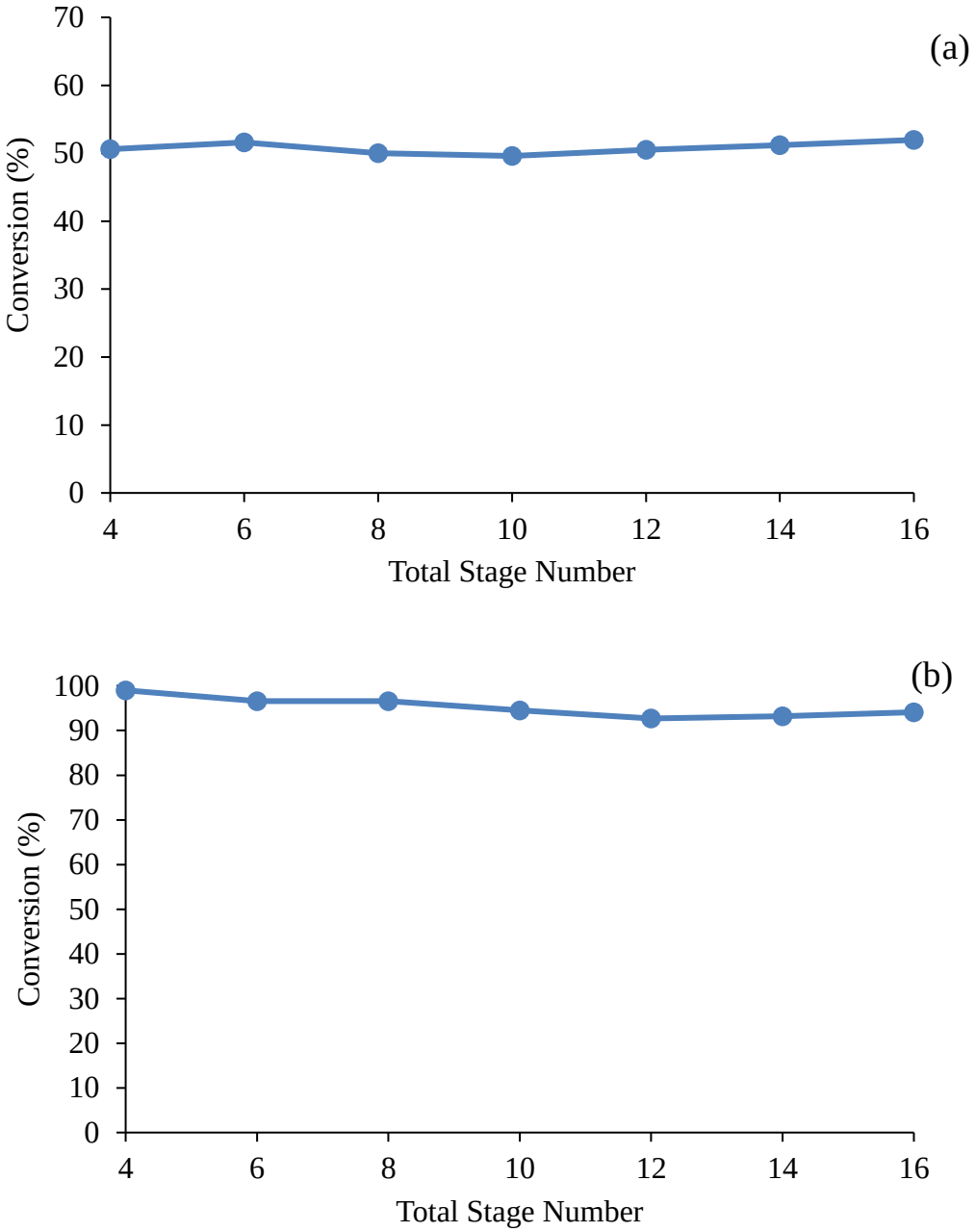

Figure 4-5 Effect of total stage number on conversion with (a) 2 mg/g and (b) 5 mg/g of CTec2 using α-cellulose as substrate. The enzyme-addition locations are set to be the (a) penultimate stage and the (b) last stage. Operation time is 200 days.

Other conditions in this simulation are set to be the same as the experimental conditions. Simulation data are presented by the markers and the lines are added to show the changing trend.

Effect of Enzyme Loading

The effect of enzyme loading on glucose concentration and conversion was simulated in the eight-stage countercurrent system (Figure 4-6). To make a fair comparison, the same enzyme-addition location (Stage 7) was used for all test points. According to Figure 4-6, as expected, both glucose concentration and conversion increase significantly as the enzyme loading increases from 1 to 6 mg/g. When the enzyme loading is 6 mg/g, the glucose concentration is 90 g/L and conversion is nearly 100%.

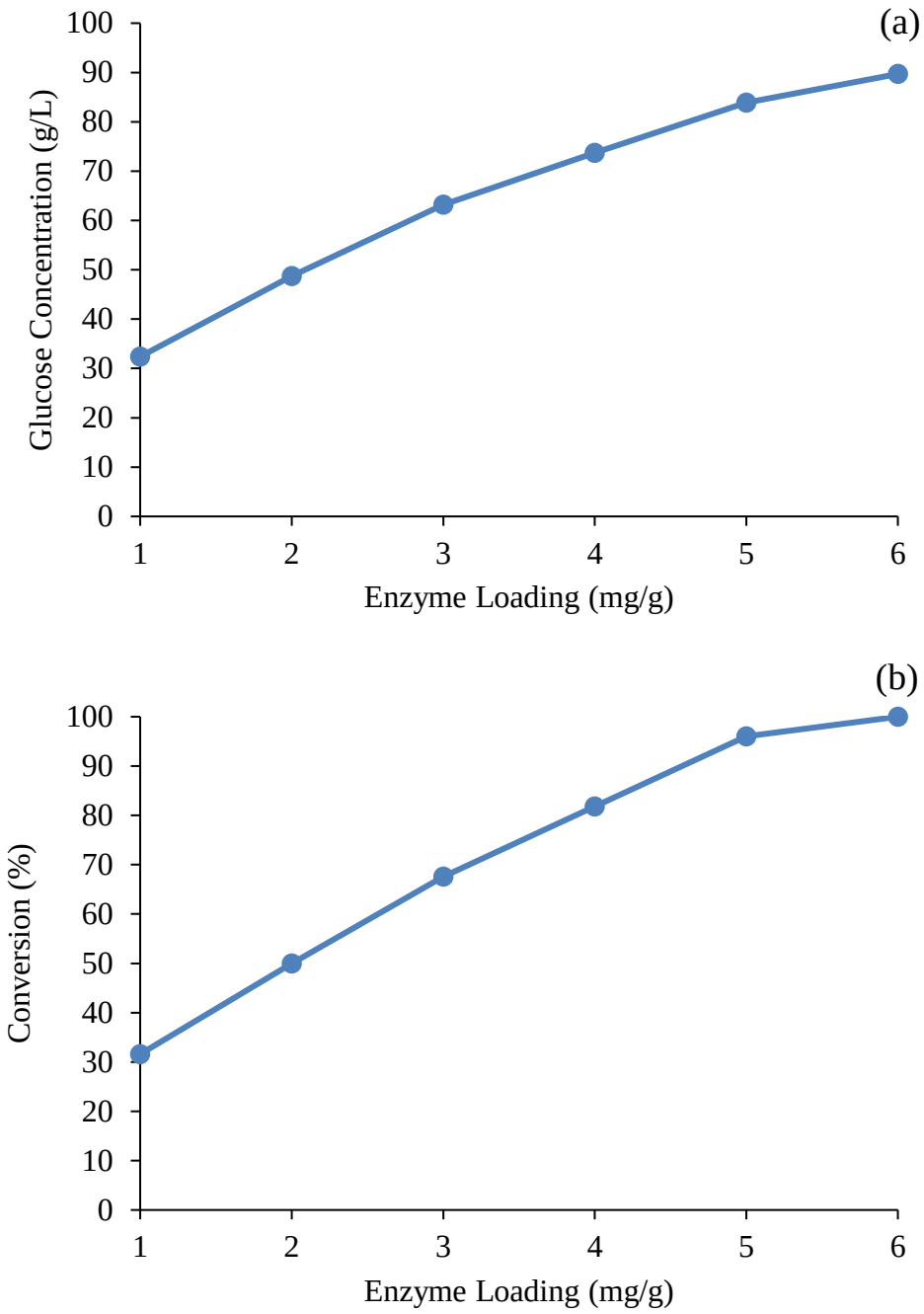

Figure 4-6 Effect of enzyme loading on (a) glucose concentration and (b) conversion in the eight-stage system using α-cellulose as substrate. Enzyme-addition location is Stage 7. Operation time is 200 days. Other conditions in this simulation are

set to be the same as the experimental conditions. Simulation data are presented by the markers and the lines are added to show the changing trend.

Effect of Liquid Residence Time and Solids Loading Rate

The LRT (Eq. 4-10) determines how long the liquid remains in the countercurrent system. A longer LRT allows higher product concentration (Fu, 2007; Holtzapple et al., 1999). To obtain various LRTs, in this study, the transfer frequency was adjusted, which corresponds to the *t* in Eq. 3-10.

$$\text{LRT (day)} = \frac{\text{total liquid volume in the system (L)}}{\text{flowrate of liquid out of the system } \left(\frac{\text{L}}{\text{day}}\right)} \tag{4-10}$$

The SLR (Eq. 4-11) represents the rate that biomass is added to the system. A lower SLR allows longer solid residence time, which is a measure of how long the solids remain in the countercurrent system. Longer solid residence times increase digestion, and therefore improve conversion (Fu, 2007; Holtzapple et al., 1999). To obtain various SLRs, in this study, during each transfer, the amount of solid feed added to Stage 1 was adjusted, which corresponds to the continuum particles ($\hat{n}(x)$) added to conversion = 0 interval in Stage 1.

$$\text{SLR } \left(\frac{\text{g}}{\text{L} \cdot \text{day}}\right) = \frac{\text{solids fed per day } \left(\frac{\text{g}}{\text{day}}\right)}{\text{total liquid volume in the system (L)}} \tag{4-11}$$

Figure 4-7 shows the CPDM "map" for countercurrent saccharification of α-cellulose at enzyme loadings of 3.5 and 5 mg/g with various LRTs and SLRs. The solid concentration in the reactors is 124 g solids/L liquid (0.11 g solids/g (solids + liquid)),

the same as the experimental concentration. As shown in Figure 4-7, as LRT increases, glucose concentration increases significantly whereas conversion decreases. As SLR decreases, conversion increases significantly whereas glucose concentration decreases. Both observations are consistent with previous studies using mixed-culture fermentation (Fu, 2007; Holtzapple et al., 1999). Furthermore, as expected, at every LRT and SLR, using enzyme loading of 5 mg/g obtains a higher glucose concentration and conversion compared to 3.5 mg/g. For enzyme loading of 5 mg/g, the "map" predicts a glucose concentration of 152 g/L and a conversion of 67% at LRT of 43 days and SLR of 4.9 g/(L·day). A glucose concentration of 83 g/L and conversion of 100% can be obtained at LRT of 43 days and SLR of 2.2 g/(L·day). A relatively high glucose concentration (>100 g/L) and high conversion (>90%) can be obtained at LRT of 43 days and SLR of 3 g/(L·day).

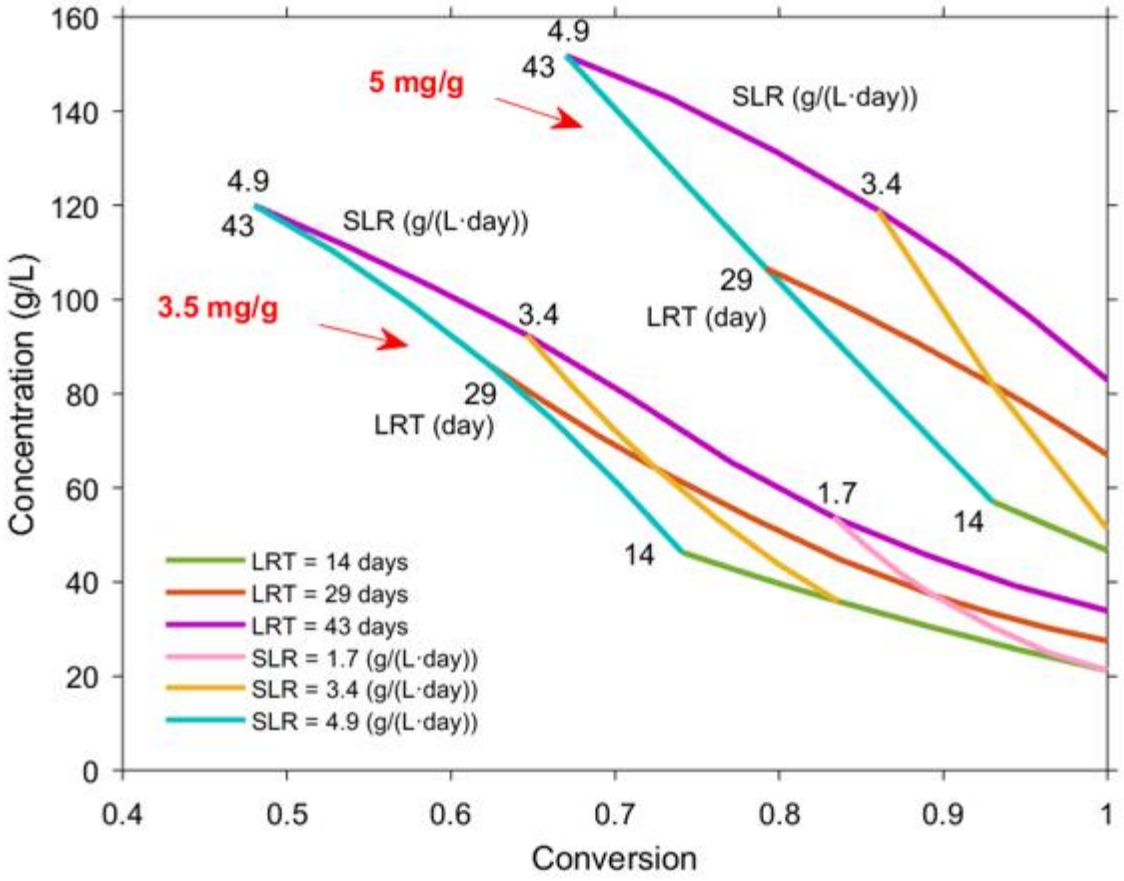

Figure 4-7 CPDM "map" for countercurrent saccharification of α-cellulose at enzyme loadings of 3.5 and 5 mg/g. Solid concentration in the reactors is 124 g solids/L liquid. Enzyme-addition location is Stage 8. Operation time is 200 days.

Figures 4-8 and 4-9 show the effect of SLR and LRT on glucose concentration, inhibition parameter *i*, and conversion of each stage. For 3.5 mg/g added to Stage 7, when using LRT of 43 days, SLR of 3.4 g/(L·day), and solid concentration of 124 g solids/L liquid, the obtained glucose concentration of Stage 1 is 93 g/L (Figure 4-8(a)).

When decreasing the LRT to 29 days and keeping SLR and solid concentration constant, the obtained glucose concentration of all stages decreases; the glucose concentration of Stage 1 decreases to 64 g/L.

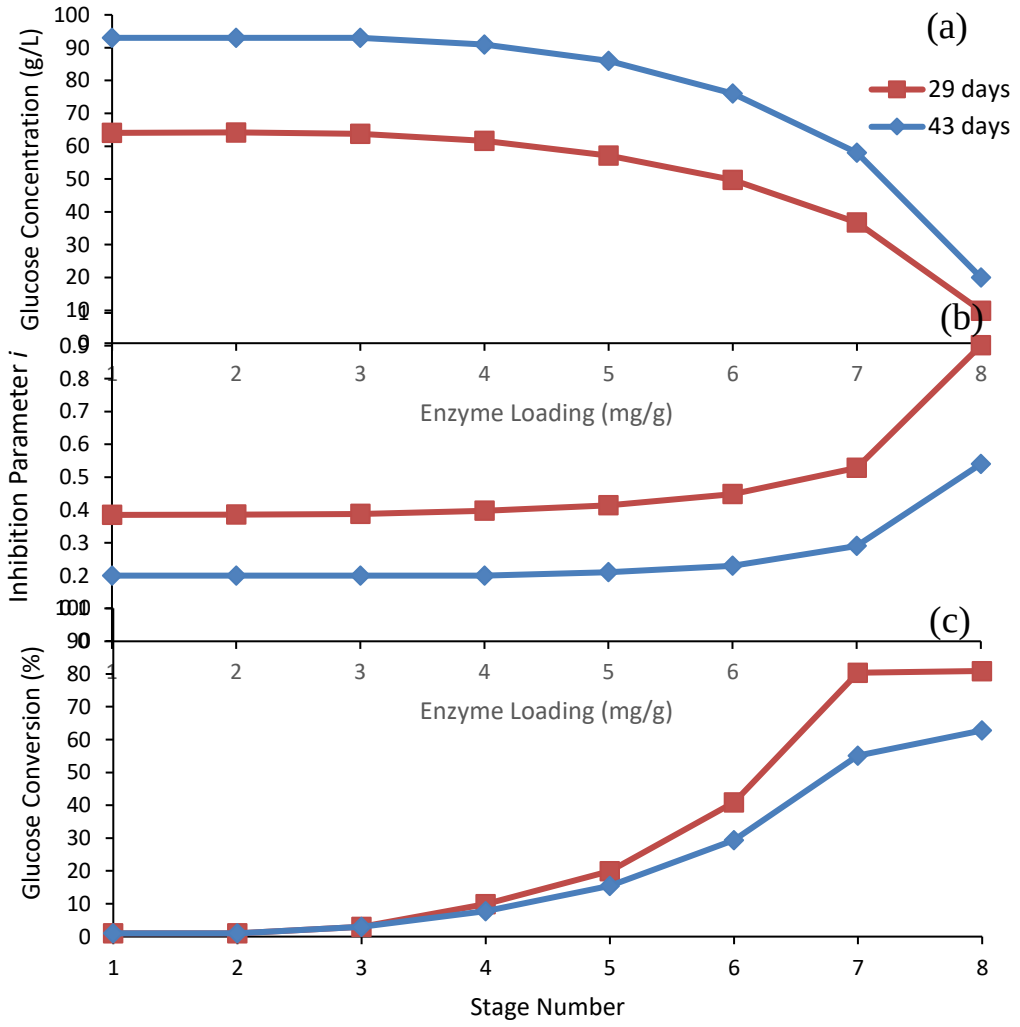

Figure 4-8 Effect of liquid residence time on (a) glucose concentration, (b) inhibition parameter *i*, and (c) conversion of each stage. Substrate is α-cellulose. Solid concentration in the reactors is 124 g solids/L liquid. Enzyme-addition location is Stage 7. Enzyme loading is 3.5 mg/g. Solids loading rate is 3.4 g/(L·day). Operation time is 200 days.

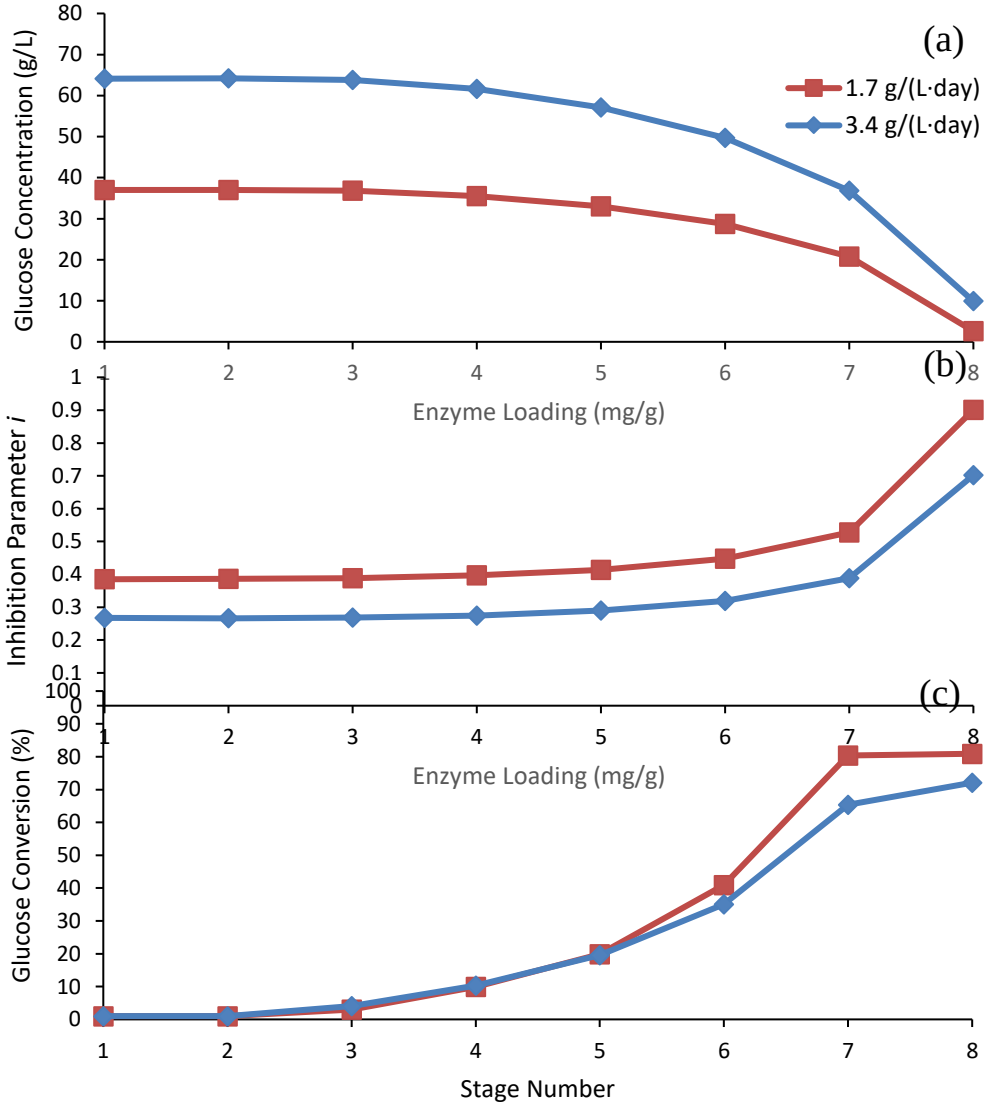

Figure 4-9 Effect of solids loading rate on (a) glucose concentration, (b) inhibition parameter *i*, and (c) conversion of each stage. Substrate is α-cellulose. Solid concentration in the reactors is 124 g solids/L liquid. Enzyme-addition location is Stage 7. Enzyme loading is 3.5 mg/g. Liquid residence time is 29 days. Operation time is 200 days.

The inhibition parameter *i* relates to glucose concentration only and represents the fraction of total enzyme that is not inhibited. At 93 g/L of glucose concentration (LRT: 43 days, Stage 1), only 20% of enzymes remain active (Figure 4-8(b)). Figures 4-8(b) and (c) show that as the inhibition parameter *i* increases, the conversion in Stages 5–8 increases significantly. (*Note:* The conversion of each stage is calculated by using particle conversion distribution function: $\text{Conversion of each stage (\%)} = \frac{1}{n_0}\int_0^1 x\hat{n}(x)dx \times 100\%$, which is different from the previously mentioned conversion for the entire reactor train.) Similar patterns are shown when increasing SLR from 1.7 to 3.4 g/(L·day) and keeping LRT (29 days) and solid concentration (124 g solids/L liquid) constant (Figure 4-9).

Comparison of Countercurrent to Batch

To evaluate the efficacy of countercurrent saccharification, an eight-stage countercurrent system is compared with batch saccharification (Figure 4-10). Batch simulations use the modified HCH-1 model, and countercurrent simulations use the CPDM model with the modified HCH-1 equation as the governing equation. To compare the enzyme requirement on an equal basis, in this section, batch and countercurrent saccharifications have the same:

(1) Conversion – Total conversion (100%) was used.

(2) Product concentration – In countercurrent saccharification, the sugar concentration in the product is based on the solid:liquid ratio added to the reactor train; therefore, the batch solid concentration (g solids/L liquid) was set equal to the

solid:liquid ratio added to the reactor train (g added solids/L added liquid) in every countercurrent transfer.

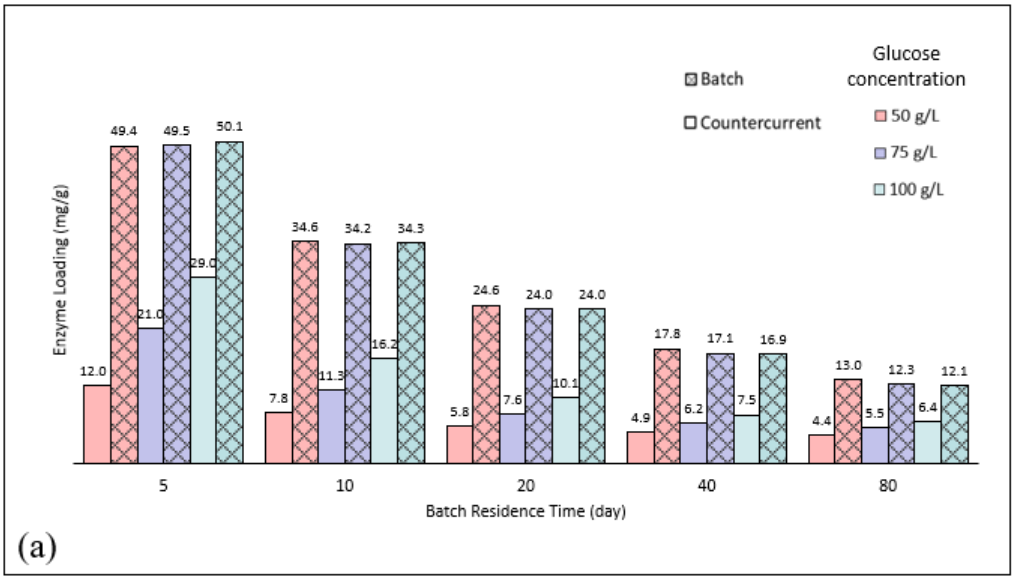

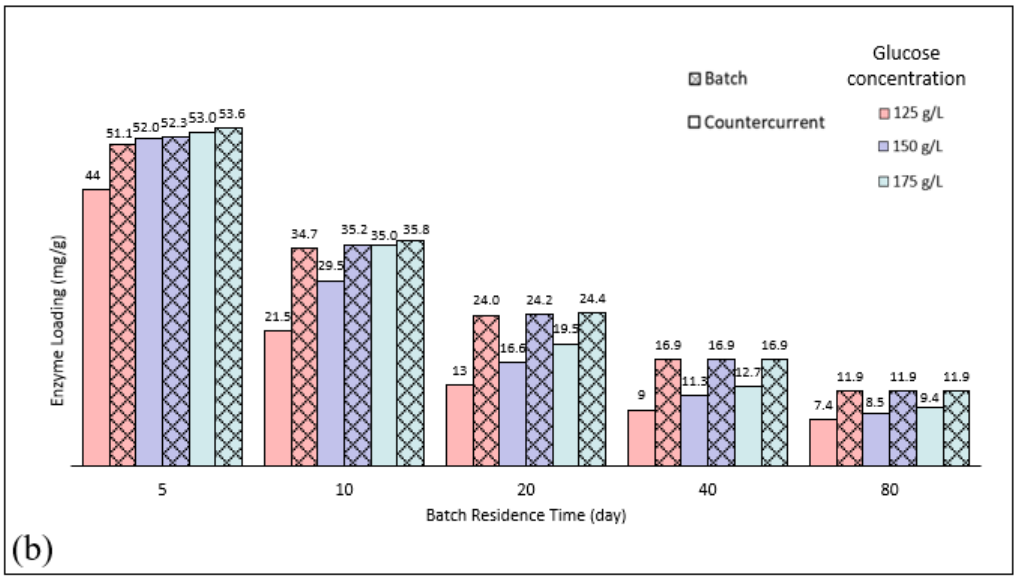

Figure 4-10 Comparison of enzyme requirements for batch and countercurrent saccharifications at various batch residence time and glucose concentrations,

(a) low glucose concentrations and (b) high glucose concentrations. The conversion of all conditions is 100%. Solid concentration in batch (g solids/L liquid) = solid:liquid ratio added to the reactor train (g added solids/L added liquid) in every countercurrent transfer. The liquid residence time in countercurrent saccharification is adjusted to reach the same batch reactor volume using the method in the previous section (Reactor volume calculation). The solid concentration in every stage in countercurrent saccharification is 250 g solids/L liquid. Enzyme-addition location is Stage 8. Operation time is 200 days. The substrate is α-cellulose. Batch simulations use the modified HCH-1 model. Countercurrent simulations use the CPDM model with the modified HCH-1 equation as the governing equation. (Note: In this section, sampling was not included in the simulation of countercurrent saccharification.)

(3) Reactor volume – This ensures the same capital cost. Using the method in the previous section (Reactor volume calculation), the LRT in countercurrent saccharification is adjusted to reach the same reactor volume as batch saccharification.

Some industrial reactors, such as percolation reactors, allow for high solid concentrations, which reduces capital costs. In this section, the solid concentration in the reactors in countercurrent saccharification was 250 g solids/L liquid (0.2 g solids/g (solids + liquid)) and the enzyme-addition location was Stage 8.

As shown in Figure 4-10, to reach 50 g glucose/L, using 5-day batch residence time, the countercurrent system reduces enzyme loadings by 4.1 times compared to

batch; however, the enzyme requirement is still more than 10 mg/g. As batch residence time increases, as expected, the enzyme requirements of all conditions decrease significantly. To reach 50 g glucose/L, at batch residence times of 40 and 80 days, the enzyme loadings of countercurrent saccharification are 4.9 and 4.4 mg/g respectively, which reduce enzyme loadings by 3.6 and 3 times compared to batch. To reach 100 g glucose/L, at batch residence times of 40 and 80 days, the enzyme loadings of countercurrent saccharification are 7.5 and 6.4 mg/g respectively, which reduce enzyme loadings by nearly 2 times compared to batch (Figure 4-10(a)). To reach 125 g glucose/L, at batch residence time of 40 days, the enzyme loading of countercurrent saccharification is 9 mg/g, which reduces enzyme loading by 1.9 times compared to batch. To reach 125, 150, and 175 g glucose/L, at batch residence time of 80 days, the enzyme loadings of countercurrent saccharification are all less than 10 mg/g, which reduce enzyme loadings by more than 1.25 times compared to batch (Figure 4-10(b)).

These results indicate that under all conditions, countercurrent saccharification requires less enzyme than batch saccharification; however, it is particularly effective at low product concentrations. In the countercurrent system, when product concentrations are high, the glucose concentrations in the first several stages are all high (such as Figure 4-8(a)). At high product concentrations, enzymes are highly inhibited and the benefits of countercurrent saccharification are less pronounced.

Conclusions

This chapter reports kinetic modeling of countercurrent saccharification. The CPDM model was used to simulate multi-stage countercurrent saccharification of α-

cellulose with the modified HCH-1 model as the governing equation. This model predicted the experimental glucose concentration and conversion with average errors of 3.5% and 4.7%, respectively, which is sufficiently accurate to determine optimal operating conditions with α-cellulose. CPDM prediction results showed that enzyme-addition location, enzyme loading, LRT, and SLR significantly affected the glucose concentration and conversion. Compared to batch saccharification at the same conversion, product concentration, and reactor volume, countercurrent saccharification is more beneficial when the product concentrations are low.

This study provides a foundation for simulating countercurrent saccharification using real-world lignocellulose as substrate. However, because of the complicated composition and structure of lignocellulose, more factors must be considered in future models, such as lignin-enzyme interaction.

CHAPTER V

TECHNO-ECONOMIC ANALYSIS OF ENZYMATIC CELLULOSE HYDROLYSIS

Introduction

As shown in Chapter IV, in countercurrent saccharification, lower product concentration and higher residence time allow lower enzyme loading to reach 100% conversion, which means lower enzyme cost. However, higher residence time usually requires larger reactor volume, which means higher capital cost; lower product concentration usually requires both higher energy consumption to get a concentrated product and larger reactor volume, which means both higher utility cost and higher capital cost. Therefore, a techno-economic analysis is necessary to determine the operating point of countercurrent saccharification that has the lowest cost of cellulosic sugar production.

In this analysis, besides countercurrent saccharification, a dewatering process that concentrates the sugar solution obtained from the saccharification process was included. The concentrated sugars can be readily transported, thereby allowing the biomass to be processed in a distributed manner. The concentrated sugars can be processed in centralized plants to make a variety of products, such as ethanol, butanol, succinic acid, and lactic acid (Liang et al., 2017).

Process Description

Figure 5-1 shows the process scheme for enzymatic hydrolysis of α-cellulose. As shown in the figure, there are two sections: (1) countercurrent saccharification –

substrate is hydrolyzed by enzyme to obtain saccharification sugar solution; (2) dewatering – saccharification sugar solution is dewatered to obtain concentrated sugar solution.

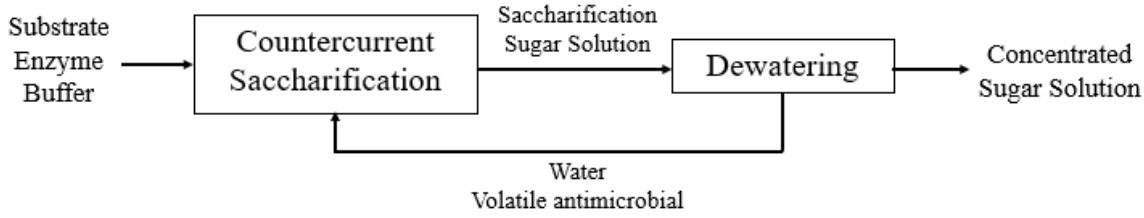

Figure 5-1 Process scheme for enzymatic hydrolysis of α-cellulose.

Countercurrent Saccharification

Figure 5-2 shows the schematic of countercurrent saccharification. Substrate, enzyme, and preheated liquid materials are added to the different locations of the reactors. In the laboratory, using multiple centrifuge bottles as reactors to achieve countercurrent movement of solids and liquids is convenient and practical. However, at industrial scale, a continuous and simpler configuration, such as a packed column (Liang et al., 2017), is envisioned for countercurrent saccharification. This study did not involve the detailed design of the countercurrent saccharification reactor. To simplify the economic analysis, unless otherwise specified, the reactor was considered as a tank. The conversion of this process was assumed to be 100%.

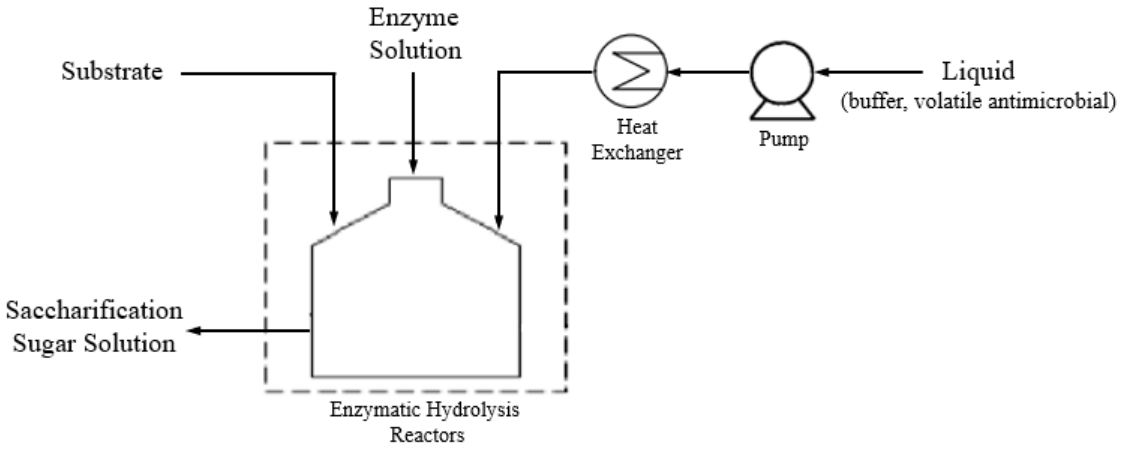

Figure 5-2 Schematic of countercurrent saccharification.

Dewatering

The dewatering process utilizes mechanical vapor recompression (MVR) evaporators, which are primarily driven by electricity and was deemed to be preferable over standard thermal (steam)-driven evaporators (Davis et al., 2013). In this study, the MVR evaporators followed National Renewable Energy Laboratory (NREL) design (Figure 5-3, Davis et al., 2013). The concentration of the concentrated sugar solution was assumed to be 909 g/L, which is saturated glucose solution at 25℃. The sugar recovery was assumed to be 100%. According to the NREL design, the operating temperature of the evaporators is kept below 80℃ to avoid possible sugar degradation at high temperatures. The electricity consumption is 0.021 kWh/kg water vaporized (Davis et al., 2013).

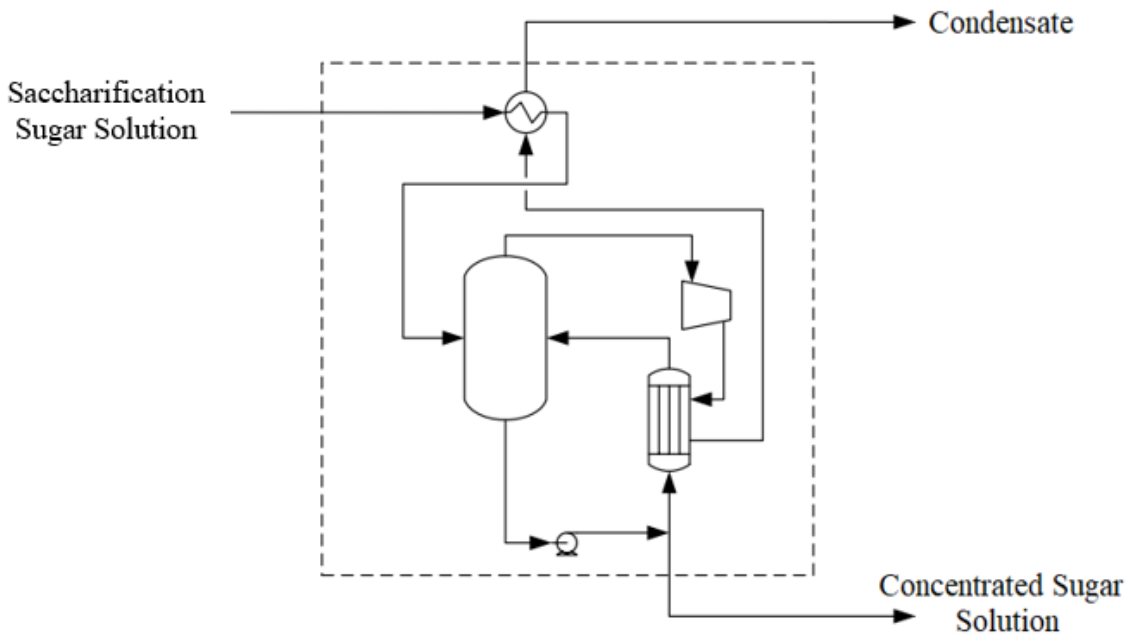

Figure 5-3 Schematic of dewatering process (Davis et al., 2013).

Cost Estimation

Fixed Capital Investment (FCI)

Countercurrent Saccharification

The purchase equipment cost mainly depends on equipment size and materials of construction. In countercurrent saccharification, equipment size is mainly affected by saccharification sugar concentration and residence time. In this study, the saccharification sugar concentration ranging from 50 g/L to 175 g/L and residence time (equivalent to batch) ranging from 5 days to 80 days were tested. The key parameters for equipment size (e.g. reactor volume, heat exchanger area, etc.) at various conditions were determined.

For the reactor material, three cases were considered: geomembrane (C1), carbon steel (C2), and stainless steel (C3). Case C1 followed the design from Granda et al. (2009), which used pile reactors made with geomembrane to perform countercurrent fermentation. The countercurrent saccharification system is similar to the countercurrent fermentation system, and Granda et al. (2009) provided the estimated FCI for the whole countercurrent fermentation process. Therefore, for this case, using Granda et al. (2009) design as the base case, the FCI of the whole countercurrent saccharification process (including reactor, pump, heat exchanger, etc.) was scaled with the scaling exponent of 0.62 based on the reactor volume. For Cases C2 and C3, after key parameters for equipment size were specified, purchase equipment costs were estimated based on matche.com. Subsequently, the FCIs were estimated by multiplying the revised Lang factor (4.3) and purchased equipment costs.

Dewatering

The equipment size in the dewatering process is mainly affected by the saccharification sugar concentration. In this study, the saccharification sugar concentration ranged from 50 g/L to 175 g/L. In the dewatering process, the saccharification sugar flowrate was considered as the key parameter for equipment size, and its value at various conditions was determined.

For the equipment material in the dewatering process, two cases were considered: carbon steel (D1) and stainless steel (D2). In the NREL design, the MVR evaporators are made with stainless steel. Therefore, for Case D2, the NREL design was considered as the base case and the purchase equipment costs at various saccharification

sugar concentrations were scaled with the scaling exponent of 0.7 based on the saccharification sugar flowrates. For Case D1, the purchase equipment costs at various conditions were obtained by using the costs in Case D2 over the materials factor (1.8). Subsequently, the FCIs were estimated by multiplying the revised Lang factor (4.3) and purchased equipment costs.

Scenarios

In the countercurrent saccharification and dewatering process, three combinations of the cases were considered:

Scenario A: Case C1 + Case D1

This scenario includes the low-cost geomembrane design and MVR evaporators made with carbon steel, which has the lowest FCI in all combinations.

Scenario B: Case C2 + Case D1

The equipment in the countercurrent saccharification and dewatering process are all made with carbon steel. This scenario has the lowest FCI in all combinations without the geomembrane design included.

Scenario C: Case C3 + Case D2

The equipment in the countercurrent saccharification and dewatering process are all made with stainless steel. This scenario has the highest FCI in all combinations.

Utility Cost (Dewatering)

The MVR evaporators are primarily driven by electricity; therefore, in this study, the utility cost of dewatering process was assumed to be equal to the electricity cost.

According to the U.S. Energy Information Agency (2018), the Texas electricity rate for industrial use in 2018 is $0.0554/kWh. Using Eq. 5-1, the utility cost (dewatering) was calculated.

$$\begin{aligned}\text{Utility Cost (\$/h)} &= \text{Electricity rate (\$/kWh)} \\ &\times \text{Electricity consumption per kg water evaporated (kWh/kg)} \\ &\times \text{Water evaporation amount per hour (kg/h)}\end{aligned} \tag{5-1}$$

Enzyme Cost

The enzyme cost depends on enzyme loading and enzyme unit price. To reach 100% conversion in countercurrent saccharification, the enzyme loadings at various conditions have been determined (Figure 4-10, Liang et al., 2019b). For enzyme unit price, four cases ranging from $1.25/kg protein to $10.14/kg protein were considered. Table 5-1 summarizes the key information.

Table 5-1 Enzyme unit price

Case	Enzyme unit price ($/kg protein)	Source
E1	6.27	CTec2 price, estimated by Liu et al., 2016.
E2	1.25	Assume cellulase protein price = soy protein price, the cheapest protein on the market.
E3	4.24	On-site cellulase production cost, cited from NREL design and Liu et al., 2016.
E4	10.14	Cellulase protein price, estimated by Klein-Marcuschamer et al., 2012.

Assumptions

Table 5-2 summarizes the assumptions for economic evaluation. In this study, the feedstock cost was not considered because α-cellulose is not a real-world substrate. The minimum selling price was determined as the summation of enzyme cost, utility cost (dewatering), depreciation, and fixed operating costs (Eq. 5-2).

$$\begin{aligned}&\text{Minimum selling price (no feedstock cost, \$/kg glucose)}\\&= \text{Enzyme Cost (\$/kg glucose)} + \text{Utility Cost (\$/kg glucose, dewatering only)}\\&+ \text{Depreciation (\$/kg glucose)}\\&+ \text{Fixed operating costs (\$/kg glucose, including local taxes, insurance, maintenance, and labor)}\end{aligned} \quad (5\text{-}2)$$

Table 5-2 Assumptions for economic evaluation

Title	**Parameter**
Plant capacity	40 dry tonne biomass/h
Plant life	20 years
Financing	100% equity
Plant operation	8000 h/year
Working capital (WC)	0.05 × FCI
Depreciation	straight-line model, 0.05/year × FCI
Local taxes	0.03/year × FCI
Insurance	0.007/year × FCI
Maintenance	0.03/year × FCI
Labor	$1.6 million/year
Dollars	Dec. 2018

Note: income tax was not included.

Results and Discussion

Minimum Selling Price

Using estimated CTec2 price (E1) as the enzyme unit price, Figure 5-4 shows the minimum selling prices at various residence time and saccharification sugar concentrations with the three scenarios. As expected, when using equipment with inexpensive materials, higher residence time and lower saccharification sugar concentration favor lower minimum selling prices. For Scenarios A, B, and C, the lowest minimum selling prices are $0.079, $0.121, and $0.160/kg glucose, respectively. Figure 5-5 shows the cost distribution of the three lowest minimum selling prices. As shown in

the figure, enzyme costs contribute most to the minimum selling prices at all three scenarios, followed by fixed operating costs. When using equipment with more expensive materials, the contributions of fixed operating costs and depreciation increase, whereas the contribution of utility costs decreases.

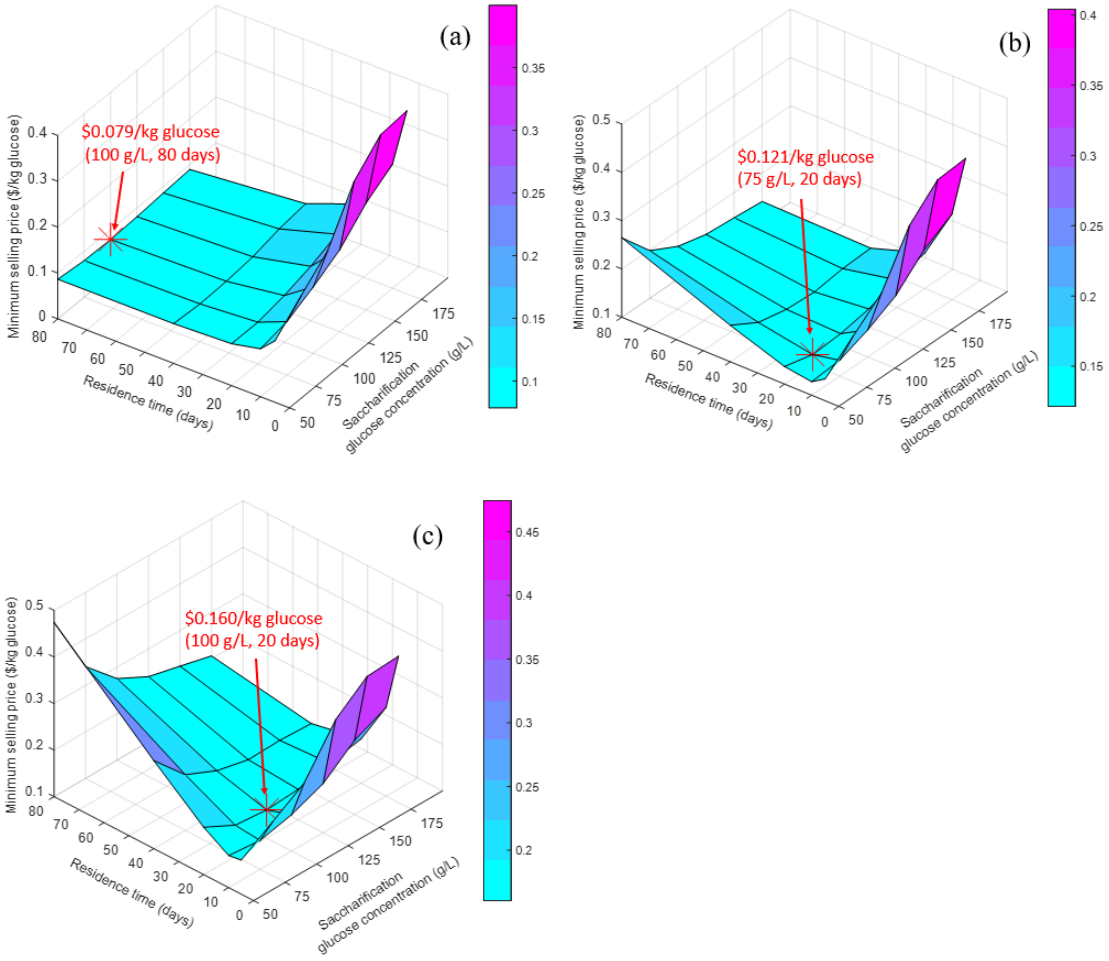

Figure 5-4 Minimum selling prices at various residence time and saccharification sugar concentrations with (a) Scenario A, (b) Scenario B, and (c) Scenario C. Lowest

minimum selling prices are presented by markers. Enzyme unit price is $6.27/kg protein (E1).

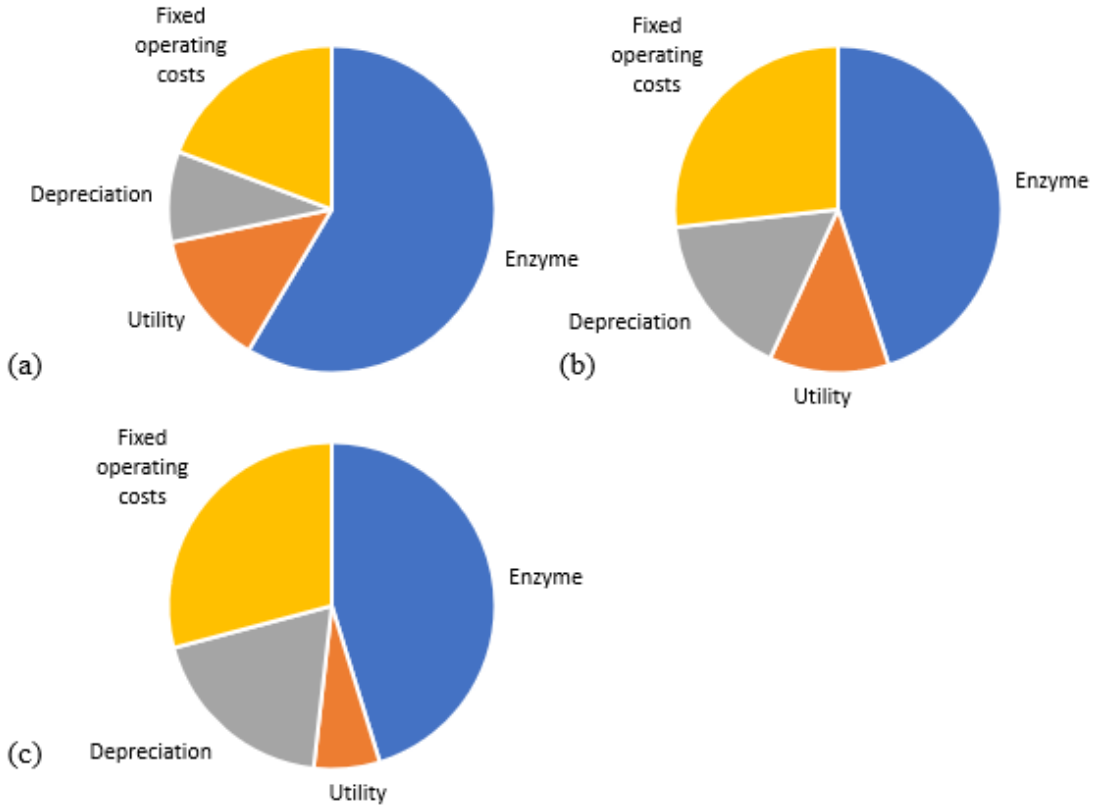

Figure 5-5 Cost distribution of the lowest minimum selling prices at (a) Scenario A (b) Scenario B, and (c) Scenario C. Enzyme unit price is $6.27/kg protein (E1).

Effect of Enzyme Unit Price

Using various enzyme unit prices and equipment materials, the minimum selling prices at various saccharification sugar concentrations and residence time were

calculated. Figure 5-6 summarizes the lowest minimum selling prices at various cases and the corresponding conditions are listed. As shown in the figure, enzyme unit price significantly affects the minimum selling price. Besides, as expected, for cases with low enzyme unit price, the lowest minimum selling prices are obtained at high saccharification sugar concentrations, which lowers the utility cost and capital cost. When the enzyme unit price was assumed to be equal to soy protein (E2), using geomembrane reactor and carbon steel MVR evaporators (Scenario A), the lowest minimum selling price is $0.036/kg glucose. When the enzyme unit price was assumed to be equal to the on-site cellulase production cost in NREL design (E3), using geomembrane reactor and carbon steel MVR evaporators (Scenario A), the lowest minimum selling price is $0.064/kg glucose; using carbon steel reactor and MVR evaporators (Scenario B), the lowest minimum selling price is $0.102/kg glucose.

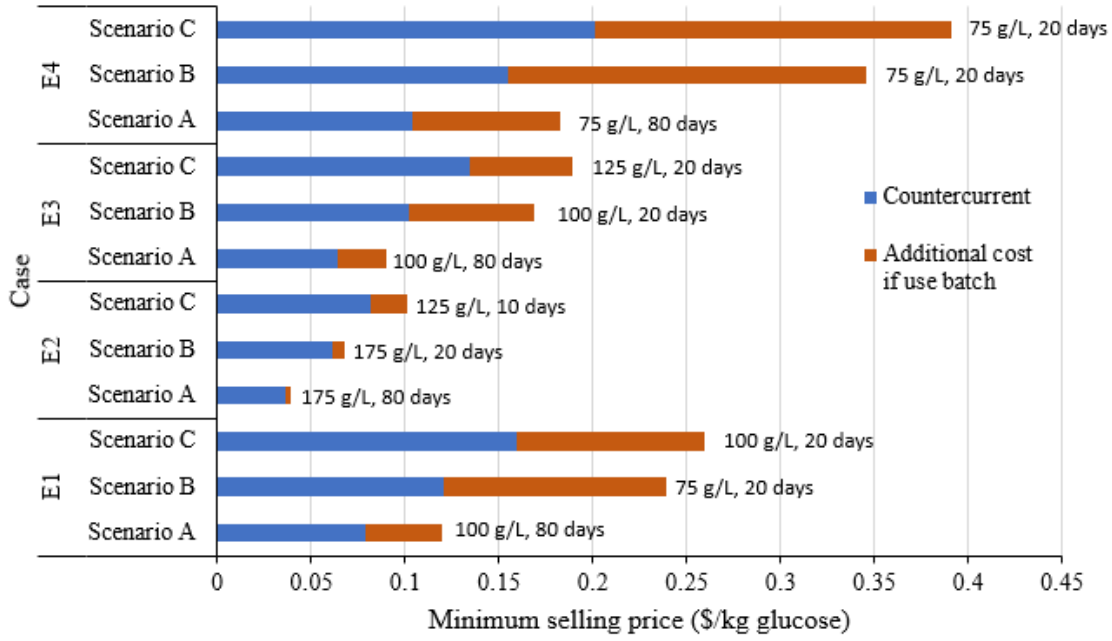

Figure 5-6 Lowest minimum selling prices at various enzyme unit prices and equipment materials with countercurrent saccharification and comparison with batch saccharification.

Effect of Return on Investment (ROI)

In this study, the total cost was determined as the summation of minimum selling price and ROI, where ROI was a factor of total capital investment (FCI + WC). Using various enzyme unit prices, equipment materials, and ROIs, the total costs at various saccharification sugar concentrations and residence time were calculated. Figure 5-7 shows the lowest total costs at various cases. As shown in the figure, ROI significantly affects the total cost. When including a 15% ROI, using geomembrane reactor and carbon steel MVR evaporators (Scenario A), the total costs are as low as $0.100/kg

glucose with estimated CTec2 price ($6.27/kg protein) and $0.082/kg glucose with on-site cellulase production cost ($4.24/kg protein).

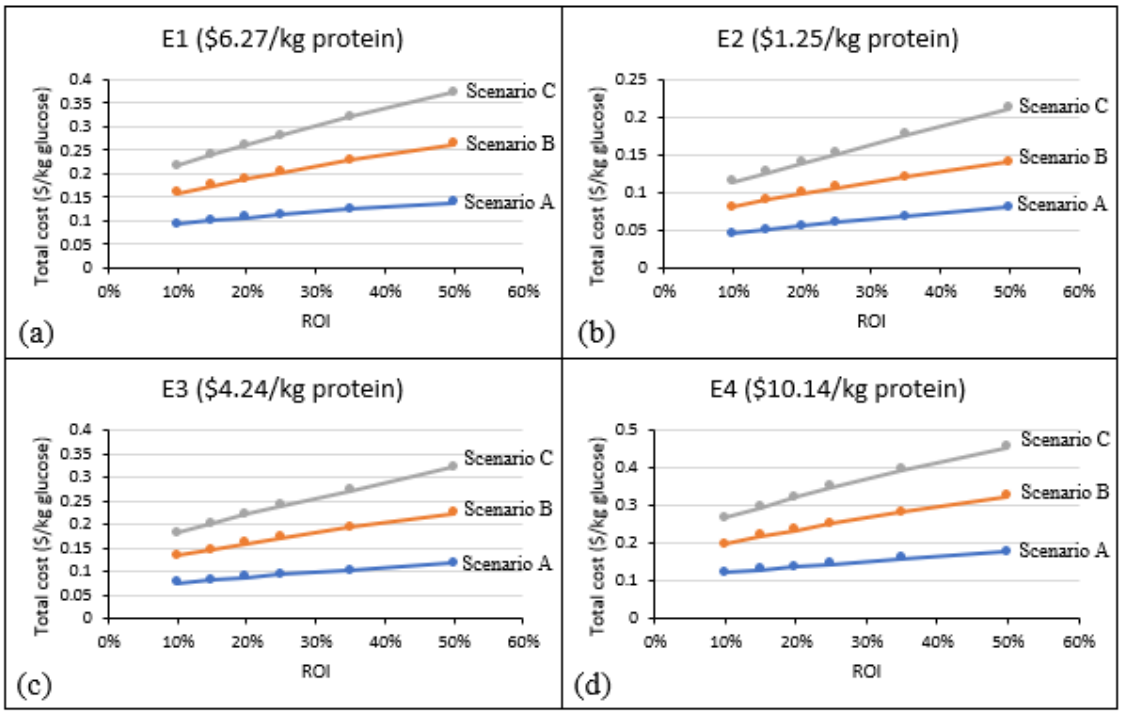

Figure 5-7 Effect of ROI on the total costs at various enzyme unit prices and equipment materials.

Comparison of Countercurrent to Batch

Figure 5-6 also shows the additional costs if using batch saccharification at the same condition, equipment material, and enzyme unit price. Generally, compared to countercurrent saccharification, batch saccharification increases the minimum selling prices significantly. For the cases with CTec2 price (E1) and on-site cellulase production

cost (E3), batch saccharifications increase the minimum selling prices by $0.022–0.10/kg glucose. As expected, higher enzyme unit prices increase the costs of sugar production. Additionally, higher enzyme costs provide more benefits of countercurrent over batch, particularly at low saccharification sugar concentrations (Chapter IV).

Conclusions

In this chapter, techno-economic analysis was performed for cellulosic sugar production, which included countercurrent saccharification and dewatering. Various reaction conditions, equipment materials, enzyme unit prices, and ROIs were considered. When including utility cost (dewatering), enzyme cost, depreciation, and fixed operating costs, using a geomembrane reactor and carbon steel MVR evaporators, the minimum selling prices are as low as $0.079/kg glucose with estimated CTec2 price ($6.27/kg protein) and $0.064/kg glucose with on-site cellulase production ($4.24/kg protein); when including an additional 15% ROI, the total costs are as low as $0.100/kg glucose and $0.082/kg glucose, respectively. Compared to batch saccharification at the same reaction conditions, equipment materials, and enzyme unit prices, countercurrent saccharification significantly reduces the cost of cellulosic sugar production.

CHAPTER VI

CONCLUSIONS

Countercurrent saccharification is a promising way to minimize enzyme loading while maintaining high conversions. Experimental results showed that using α-cellulose as substrate, to reach a given glucose conversion compared to typical (5-day) batch saccharification, countercurrent saccharification reduced enzyme loadings by 8–16.8 times. The great reduction resulted from the inherent benefits of countercurrent saccharification as well as a longer residence time. Using pretreated corn stover as substrate, to reach a given glucose conversion compared to typical (5-day) batch saccharification, countercurrent saccharification reduced enzyme loadings up to 1.9 times. However, in countercurrent saccharification experiments, 3–4 months are usually required to acquire a single steady-state data point. To save time and labor, simulation of this process is necessary to test various reaction conditions and determine the optimal operating point.

In this study, α-cellulose was used for modeling because of its simpler composition compared to real-world lignocellulose, which contains lignin. Lignin is known to bind cellulase enzymes non-productively (Kumar and Wyman, 2009b), which complicates the kinetic modeling.

To simulate countercurrent saccharification, a kinetic model that can accurately predict batch saccharification under various reaction conditions is necessary. This study modified the HCH-1 model to extend its application to integrated batch enzymatic hydrolysis; it performed well when fitting 10-day batch cellulose hydrolysis at various

experimental conditions. Local and global sensitivity analyses were performed to determine the controlling parameters at different hydrolysis stages. Mechanistic (and semi-mechanistic) literature models for long-term batch enzymatic hydrolysis were compared with the modified HCH-1 model and evaluated by AICc. Comparison results show that the modified HCH-1 model provides the best description of enzymatic cellulose hydrolysis.

To simulate multi-stage countercurrent saccharification of α-cellulose, the CPDM model was used with the modified HCH-1 model as the governing equation. This model predicted the experimental glucose concentration and conversion with average errors of 3.5% and 4.7%, respectively, which is sufficiently accurate to determine optimal operating conditions with α-cellulose. CPDM prediction results showed that enzyme-addition location, enzyme loading, LRT, and SLR significantly affected the glucose concentration and conversion. Compared to batch saccharification at the same conversion, product concentration, and reactor volume, countercurrent saccharification is more beneficial when the product concentrations are low.

Techno-economic analysis was performed for cellulosic sugar production, which included countercurrent saccharification and dewatering. Various reaction conditions, equipment materials, enzyme unit prices, and ROIs were considered. When including utility cost (dewatering), enzyme cost, depreciation, and fixed operating costs, using geomembrane reactor and carbon steel MVR evaporators, the minimum selling prices are as low as $0.079/kg glucose with estimated CTec2 price ($6.27/kg protein) and $0.064/kg glucose with on-site cellulase production cost ($4.24/kg protein); when

including an additional 15% ROI, the total costs are as low as $0.100/kg glucose and $0.082/kg glucose, respectively. Compared to batch saccharification at the same reaction conditions, equipment materials, and enzyme unit prices, countercurrent saccharification significantly reduces the cost of cellulosic sugar production.

REFERENCES

Bansal P, Hall M, Realff MJ, Lee JH, Bommarius AS. Modeling cellulase kinetics on lignocellulosic substrates. Biotechnol Adv. 2009;27:833–48.

Bommarius AS, Katona A, Cheben SE, Patel AS, Ragauskas AJ, Knudson K, Pu Y. Cellulase kinetics as a function of cellulose pretreatment. Metab Eng. 2008;10:370–81.

Brown RF, Holtzapple MT. Parametric analysis of the errors associated with the Michaelis–Menten equation. Biotechnol Bioeng. 1990;36:1141–50.

Brown RF, Agbogbo FK, Holtzapple MT. Comparison of mechanistic models in the initial rate enzymatic hydrolysis of AFEX-treated wheat straw. Biotechnol Biofuels. 2010;3:6.

Cruys-Bagger N, Alasepp K, Andersen M, Ottesen J, Borch K, Westh P. Rate of threading a cellulose chain into the binding tunnel of a cellulase. J Phys Chem B. 2016;120:5591–600.

Darvekar P, Liang C, Karim MN, Holtzapple MT. Effect of headspace gas composition on carboxylate production in mixed-culture fermentation of corn stover. Biomass Bioenerg. 2019;126:57–61.

Darvekar P, Holtzapple MT. Assessment of shock pretreatment of corn stover using the carboxylate platform. Appl Biochem Biotechnol. 2016;178:1081–94.

Davis R, Tao L, Tan EC, Biddy MJ, Beckham GT, Scarlata C, Jacobson J, Cafferty K, Ross J, Lukas J, Knorr D. Process design and economics for the conversion of lignocellulosic biomass to hydrocarbons: dilute-acid and enzymatic deconstruction of biomass to sugars and biological conversion of sugars to hydrocarbons. National Renewable Energy Lab.(NREL), Golden, CO, United States. 2013.

Drissen RE, Maas RH, Van Der Maarel MJ, Kabel MA, Schols HA, Tramper J, Beeftink HH. A generic model for glucose production from various cellulose sources by a commercial cellulase complex. Biocatal Biotransformation. 2007;25:419–29.

Falls M, Madison M, Liang C, Karim MN, Sierra-Ramirez R, Holtzapple MT. Mechanical pretreatment of biomass – Part II: Shock treatment. Biomass Bioenerg. 2019;126:47–56.

Falls M, Meysing D, Liang C, Karim MN, ...and Holtzapple MT. Development of highly digestible animal feed from lignocellulosic biomass Part 2: Oxidative lime pretreatment (OLP) and shock treatment of corn stover. Transl Anim Sci. 2017a;1:215–20.

Falls M, Meysing D, Lonkar S, Liang C, Karim MN, Carstens G, Tedeschi LO, Holtzapple MT. Development of highly digestible animal feed from lignocellulosic biomass Part 1: Oxidative lime pretreatment (OLP) and ball milling of forage sorghum. Transl Anim Sci, 2017b;1:208–14.

Fan LT, Lee YH. Kinetic studies of enzymatic hydrolysis of insoluble cellulose: Derivation of a mechanistic kinetic model. Biotechnol Bioeng. 1983;25:2707–33.

Fenila F, Shastri Y. Optimal control of enzymatic hydrolysis of lignocellulosic biomass. Resource-Efficient Technol. 2016;2:S96–104.

Fox D, Dunn NW, Gray PP, Marsden WL. Saccharification of bagasse using a counter-current plug-flow reactor. J Chem Technol Biot. 1983;33:114-8.

Fu Z, Holtzapple MT. Anaerobic mixed-culture fermentation of aqueous ammonia-treated sugarcane bagasse in consolidated bioprocessing. Biotechnol Bioeng. 2010a;106:216–27.

Fu Z, Holtzapple MT. Consolidated bioprocessing of sugarcane bagasse and chicken manure to ammonium carboxylates by a mixed culture of marine microorganisms. Bioresour Technol. 2010b;101:2825–36.

Fu Z, Holtzapple MT. Fermentation of sugarcane bagasse and chicken manure to calcium carboxylates under thermophilic conditions. Appl Biochem Biotechnol. 2010c;162:561–78.

Fu Z. Conversion of sugarcane bagasse to carboxylic acids under thermophilic conditions. PhD diss., Texas A & M University, College Station, TX (US); 2007.

Granda CB, Holtzapple MT, Luce G, Searcy K, Mamrosh DL. Carboxylate platform: the MixAlco process part 2: process economics. Appl Biochem Biotechnol. 2009;156:107–24.

Gusakov AV, Sinitsyn AP, Klyosov AA. Kinetics of the enzymatic hydrolysis of cellulose: 1. A mathematical model for a batch reactor process. Enzyme Microb Technol. 1985;7:346–52.

Holtzapple MT, Caram HS, Humphrey AE. The HCH-1 model of enzymatic cellulose hydrolysis. Biotechnol Bioeng. 1984;26:775–80.

Holtzapple M, Cognata M, Shu Y, Hendrickson C. Inhibition of *Trichoderma reesei* cellulase by sugars and solvents. Biotechnol Bioeng. 1990;36:275–87.

Holtzapple MT, Davison RR, Ross MK, Aldrett-Lee S, Nagwani M, Lee CM, et al. Biomass conversion to mixed alcohol fuels using the MixAlco process. Appl Biochem Biotechnol. 1999;77–9:609–31.

Holtzapple MT, Novel mechanical pretreatment for lignocellulosic feedstocks. DOE Project DE – EE 00050005.00, College Station, TX, 2014.

Hong J, Ye X, Zhang YH. Quantitative determination of cellulose accessibility to cellulase based on adsorption of a nonhydrolytic fusion protein containing CBM and GFP with its applications. Langmuir. 2007;23:12535–40.

Jeffries TW, Schartman R. Bioconversion of secondary fiber fines to ethanol using counter-current enzymatic saccharification and co-fermentation. Appl Biochem Biotechnol. 1999;78:435-44.

Jeoh T, Cardona MJ, Karuna N, Mudinoor AR, Nill J. Mechanistic kinetic models of enzymatic cellulose hydrolysis—a review. Biotechnol Bioeng. 2017;114:1369–85.

Kadam KL, Rydholm EC, McMillan JD. Development and validation of a kinetic model for enzymatic saccharification of lignocellulosic biomass. Biotechnol Prog. 2004;20:698–705.

Klass D L. Biomass for renewable energy and fuels. Encyclopedia of Energy, 2004, 1(1): 193-212.

Klein-Marcuschamer D, Oleskowicz-Popiel P, Simmons BA, Blanch HW. The challenge of enzyme cost in the production of lignocellulosic biofuels. Biotechnol Bioeng. 2012;109:1083–7.

Kumar R, Wyman CE. An improved method to directly estimate cellulase adsorption on biomass solids. Enzyme Microb Technol. 2008;42:426–33.

Kumar R, Wyman CE. Cellulase adsorption and relationship to features of corn stover solids produced by leading pretreatments. Biotechnol Bioeng. 2009a;103:252–67.

Kumar R, Wyman CE. Does change in accessibility with conversion depend on both the substrate and pretreatment technology? Bioresour Technol. 2009b;100:4193–202.

Liang C. Batch enzymatic hydrolysis of pretreated corn stover and improvements with countercurrent saccharification. MS thesis, Texas A & M University, College Station, TX (US); 2015.

Liang C, Lonkar S, Darvekar P, Bond A, Zentay AN, Holtzapple MT, et al. Countercurrent enzymatic saccharification of pretreated corn stover Part 2: Lime

+ shock pretreated corn stover and commercial approach. Biomass Bioenerg. 2017;97:43–52.

Liang C, Gu C, Raftery J, Karim MN, Holtzapple M. Development of modified HCH-1 kinetic model for long-term enzymatic cellulose hydrolysis and comparison with literature models. Biotechnol Biofuels. 2019a;12:34.

Liang C, Gu C, Karim MN, Holtzapple M. Kinetic modelling of countercurrent saccharification. Biotechnol Biofuels. 2019b;12:179.

Liao W, Liu Y, Wen Z, Frear C, Chen S. Kinetic modeling of enzymatic hydrolysis of cellulose in differently pretreated fibers from dairy manure. Biotechnol Bioeng. 2008;101:441–51.

Liu G, Zhang J, Bao J. Cost evaluation of cellulase enzyme for industrial-scale cellulosic ethanol production based on rigorous Aspen Plus modeling. Bioprocess Biosyst Eng. 2016;39:133–40.

Loescher ME. Volatile fatty acid fermentation of biomass and kinetic modeling using the CPDM method. PhD diss., Texas A & M University, College Station, TX (US); 1996.

Lonkar S, Liang C, Bond A, Darvekar P, Brooks H, Derner J, et al. Countercurrent saccharification of lime-pretreated corn stover–Part 1. Biomass Bioenerg. 2017;96:28–37.

Lynd LR, Laser MS, Bransby D, Dale BE, Davison B, Hamilton R, Himmel M, Keller M, McMillan JD, Sheehan J, Wyman CE. How biotech can transform biofuels. Nat Biotechnol. 2008;26:169–172.

Lynd LR, Liang X, Biddy MJ, Allee A, Cai H, Foust T, Himmel ME, Laser MS, Wang M, Wyman CE. Cellulosic ethanol: status and innovation. Curr Opin Biotechnol. 2017;45:202–11.

Macrotrends: Sugar Prices - 37 Year Historical Chart. https://www.macrotrends.net/2537/sugar-prices-historical-chart-data (2019). Accessed 1 Jun 2019.

Madison MJ, Coward-Kelly G, Liang C, Karim MN, Falls M, Holtzapple MT. Mechanical pretreatment of biomass – Part I: Acoustic and hydrodynamic cavitation. Biomass Bioenerg. 2017;98:135–41.

Martin AJP, Synge RLM. Separation of the higher monoamino-acids by countercurrent liquid-liquid extraction: the amino-acid composition of wool. Biochem J. 1941;35:91.

Nidetzky B, Steiner W. A new approach for modeling cellulase–cellulose adsorption and the kinetics of the enzymatic hydrolysis of microcrystalline cellulose. Biotechnol Bioeng. 1993;42:469–79.

Novozymes: Cellulosic ethanol - Novozymes Cellic® CTec2 and HTec2 - Enzymes for hydrolysis of lignocellulosic. 2010. http://www.shinshu-u.ac.jp/faculty/engineering/chair/chem010/manual/Ctec2.pdf. Accessed 29 Sep

2018.

Novozymes. Cellulosic ethanol - Novozymes Cellic® CTec3. 2012a. https://s3.amazonaws.com/zanran_storage/bioenergy.novozymes.com/ContentPages/2546502386.pdf. Accessed 30 Jul 2019.

Novozymes. Cellulosic ethanol - Novozymes Cellic® HTec3. 2012b. https://www.yumpu.com/en/document/read/30214569/novozymes-cellicar-htec3. Accessed 30 Jul 2019.

Ordoñez MC, Raftery JP, Jaladi T, Chen X, Kao K, Karim MN. Modelling of batch kinetics of aerobic carotenoid production using *Saccharomyces cerevisiae*. Biochem Eng J. 2016;114:226–36.

Peri S, Karra S, Lee YY, Karim MN. Modeling intrinsic kinetics of enzymatic cellulose hydrolysis. Biotechnol Prog. 2007;23:626–37.

Pham V, Holtzapple M, El-Halwagi M. Techno-economic analysis of biomass to fuel conversion via the MixAlco process. J Ind Microbiol Biotechnol. 2010;37:1157–68.

Philippidis GP, Smith TK, Wyman CE. Study of the enzymatic hydrolysis of cellulose for production of fuel ethanol by the simultaneous saccharification and fermentation process. Biotechnol Bioeng. 1993;41:846–53.

Rosales-Calderon O, Trajano HL, Duff SJ. Stability of commercial glucanase and β-glucosidase preparations under hydrolysis conditions. PeerJ. 2014;2:e402.

Rosales-Calderon O, Trajano HL, Posarac D, Duff SJ. Modeling of oxygen delignified wheat straw enzymatic hydrolysis as a function of hydrolysis time, enzyme concentration, and lignin content. Ind Biotechnol. 2016;12:176–86.

Ross MK. Production of acetic acid from waste biomass. PhD diss., Texas A & M University, College Station, TX (US); 1998.

Satari B, Karimi K, Kumar R. Cellulose solvent-based pretreatment for enhanced second-generation biofuel production: a review. Sustain Energ Fuels. 2019;3:11–62.

Selig M, Weiss N, Ji Y. Enzymatic saccharification of lignocellulosic biomass. NREL/TP-510-42629. National Renewable Energy Laboratory, Golden, CO, 2008.

Shang BZ, Chang R, Chu JW. Systems-level modeling with molecular resolution elucidates the rate-limiting mechanisms of cellulose decomposition by cellobiohydrolases. J Biol Chem. 2013;288:29081–9.

Shen J, Agblevor FA. Kinetics of enzymatic hydrolysis of steam-exploded cotton gin waste. Chem Eng Commun. 2008;195:1107–21.

Shi J, Wu D, Zhang L, Simmons BA, Singh S, Yang B, Wyman CE. Dynamic changes of substrate reactivity and enzyme adsorption on partially hydrolyzed cellulose. Biotechnol Bioeng. 2017;114:503–15.

Sobol IM. Global sensitivity indices for nonlinear mathematical models and their Monte Carlo estimates. Math Comput Simul. 2001;55:271–80.

South CR, Lynd LR. Analysis of conversion of particulate biomass to ethanol in continuous solids retaining and cascade bioreactors. Appl Biochem Biotechnol. 1994;45:467.

Thanakoses P, Black AS, Holtzapple MT. Fermentation of corn stover to carboxylic acids. Biotechnol Bioeng. 2003;83:191–200.

The Engineering Toolbox. https://www.engineeringtoolbox.com/density-aqueous-solution-organic-sugar-alcohol-concentration-d_1954.html. Accessed Apr 2019.

Uozu H, Naitoh A, Numaguchi T. Countercurrent heat exchange: U.S. Patent 4849187. 1989-7-18.

U.S. Energy Information Administration. https://www.eia.gov/electricity/. Last accessed: Sep. 10, 2019.

Wallace J, Brienzo M, García-Aparicio MP, Görgens JF. Lignin enrichment and enzyme deactivation as the root cause of enzymatic hydrolysis slowdown of steam pretreated sugarcane bagasse. New Biotechnol. 2016;33:361–71.

Wallace R, Ibsen K, McAloon A, Yee W. Feasibility study for co-locating and integrating ethanol production plants from corn starch and lignocellulosic feedstocks (revised). NREL/TP-510-37092. National Renewable Energy Lab., Golden, CO, 2005.

Wooley R, Ruth M, Glassner D, Sheehan J. Process design and costing of bioethanol technology: a tool for determining the status and direction of research and development. Biotechnol Prog. 1999;15:794–803

Yang B, Willies DM, Wyman CE. Changes in the enzymatic hydrolysis rate of Avicel cellulose with conversion. Biotechnol Bioeng. 2006;94:1122–8.

Zentay AN, Liang C, Lonkar S, Holtzapple MT. Countercurrent enzymatic saccharification of cellulosic biomass. Biomass Bioenerg. 2016;90:122–30.

Zhang Y, Xu JL, Xu HJ, Yuan ZH, Guo Y. Cellulase deactivation based kinetic modeling of enzymatic hydrolysis of steam-exploded wheat straw. Bioresour Technol. 2010;101:8261–6.

Zhou J, Wang YH, Chu J, Luo LZ, Zhuang YP, Zhang SL. Optimization of cellulase mixture for efficient hydrolysis of steam-exploded corn stover by statistically designed experiments. Bioresour Technol. 2009;100:819–25.

APPENDIX A DEVELOPMENT OF EQ. 3-3

The core structure of Eq. 3-3 was inspired by the empirical equation for batch fermentation (Eq. A-1, Fu and Holtzapple (2010a)), where sugarcane bagasse and chicken manure were anaerobically fermented to carboxylic acids.

$$\hat{r} = \frac{e(1-x)^f}{1 + g(\phi \cdot Aceq)^h} \tag{A-1}$$

where,

x is the fraction conversion of volatile solid

e, *f*, *g*, and *h* are the empirical constants

ϕ is the ratio of total grams of carboxylic acid to total grams of acetic acid equivalents (*Aceq*).

This equation relates the specific reaction rate $\hat{r}$(*x*, *Aceq*) with *Aceq* concentration and conversion (*x*). The term (1 − *x*) is described as the "conversion penalty function," which means the reaction rate decreases as the substrate is converted (South and Lynd, 1994; Fu and Holtzapple, 2010a). The denominator term describes the inhibitory effect of product (*Aceq*) on reaction rate.

To model enzymatic hydrolysis process, Eq. A-1 was modified to Eq. A-2 with the following two major adjustments: (1) the effect of enzyme concentration $[E]$, and (2) the effect of substrate concentration $[G_x^0]$.

$$\frac{d[G_1]}{dt} = \frac{e([G_x^0](1-x))^f([E])^c}{1 + g[G_1]^h} \tag{A-2}$$

Solving Eq. 4-3, taking $[E] = [E_0]$ (g/L) at $t = 0$ yields:

$$[E] = \frac{[E_0]\left(k_2[E_0] + k_1\exp\left(-t(k_1 + k_2[E_0])\right)\right)}{k_1 + k_2[E_0]} \quad \text{(A-3)}$$

Eq. A-4 can be obtained by replacing the term [E] in Eq. A-2 with Eq. A-3.

$$\frac{d[G_1]}{dt} = \frac{e([G_x^0](1-x))^f \left(\frac{[E_0]\left(k_2[E_0] + k_1\exp\left(-t(k_1 + k_2[E_0])\right)\right)}{k_1 + k_2[E_0]}\right)^c}{1 + g[G_1]^h} \quad \text{(A-4)}$$

The optimal values of the parameters *e*, *f*, *g*, *h*, *c*, k_1, and k_2 were determined by fitting the experimental data of the 16 enzymatic hydrolysis conditions (Section: Experiments for model fitness) with Eq. A-4 simultaneously. Eq. 3-3 was obtained by replacing the parameters in Eq. A-4 with the optimal values.